DEVELOPMENT OF BIODEGRADABLE MAGNESIUM ALLOYS

BY

MIR THAUFEEQUL ISLAM

A Thesis Presented to the
DEANSHIP OF GRADUATE STUDIES

KING FAHD UNIVERSITY OF PETROLEUM & MINERALS

DHAHRAN, SAUDI ARABIA

In Partial Fulfillment of the
Requirements for the Degree of

MASTER OF SCIENCE

In

MECHANICAL ENGINEERING

April 2019

KING FAHD UNIVERSITY OF PETROLEUM & MINERALS

DHAHRAN- 31261, SAUDI ARABIA

DEANSHIP OF GRADUATE STUDIES

This thesis, written by **Mir Thaufeequl Islam** under the direction of his thesis advisor and approved by his thesis committee, has been presented and accepted by the Dean of Graduate Studies, in partial fulfillment of the requirements for the degree of **MASTER OF SCIENCE IN MECHANICAL ENGINEERING.**

Dr. Syed Fida Hassan
(Advisor)

Dr. Khaled S. Al-Athel
Department Chairman

Dr. Nasser Al-Aqeeli
(Member)

Dr. Salam A. Zummo
Dean of Graduate Studies

Dr. Saheb Nouari
(Member)

18/6/2019
Date

Dedicated to my father, mother, wife, son and family.

ACKNOWLEDGMENTS

All Praises be to Allaah, the One and Only Creator and Sustainer by Whose Mercy it is that I and this work have come to be. May I always be amongst the most grateful to The Most High for everything that has been bestowed upon me.

My heart-felt appreciation and gratitude to the Kingdom of Saudi Arabia, and KFUPM for awarding me with the scholarship under which this work has been produced. May the brotherly relationship between the people of Saudi Arabia and Maldives be always strong and prosperous.

I would like to express my gratitude to Dr. Fida, Syed H., under whose supervision I have completed this thesis and whose advise I have followed to the best of my ability. And I would also like to thank my Thesis committee members Dr. Saheb Nouari and Dr. Nasser Al Aqeeli for their constructive input and feedback. Furthermore, I would like to thank lecturers, Mr. Faheemuddeen Patel and Mr. Murtaza Beig for their assistance during the compaction and extrusion phase of the experiments. In addition, my thanks and gratitude are also owed to Mr. Nasiruddin Ogunlakin, Lab Engineer Mr. Latheef Hashmi and Lab Technician Mr. Abdullaah and Mr. Abdul Aziz of the XRD lab for their kind help and assistance in the course of this research. Especially I owe my thanks to Mr. Ahmed Al-Ghanim (Materials Processing Lab) for his dedication to quality work.

My thanks also go to the CEO and the staff of State Electric Company Ltd., Maldives, for their understanding and co-operation during the term of my study leave.

Last but not least, I would like to thank my family, for whose support, patience and prayers, without which I would not have been able to continue my work.

TABLE OF CONTENTS

LIST OF TABLES

LIST OF FIGURES

LIST OF ABBREVIATIONS

SBF	:	Simulated Body Fluid
TYS	:	Tensile Yield Strength
UTS	:	Ultimate Tensile Strength
CYS	:	Compressive Yield Strength
UCS	:	Ultimate Compressive Strength
XRD	:	X-Ray Dispersive spectrum
DRX	:	Dynamic Recrystallization
BPS	:	Blend-Press-Sinter
BPS+E	:	Blend-Press-Sinter followed by Extrusion
SEM	:	Scanning Electron Microscope
FESEM	:	Field Emission Scanning Electron Microscope
ZX	:	Mg Alloy system containing Zinc and Calcium

ABSTRACT

Full Name : Mir Thaufeequl Islam

Thesis Title : Development of biodegradable Mg Alloys by extrusion

Major Field : Mechanical Engineering

Date of Degree : April 2019

The challenges faced with the use of Mg as a biodegradable metal for medical implants resulting from its high degradation rate is overcome by alloying it with other metals. This Thesis carries out the task of the development of biodegradable Mg alloys consisting of Zn, Ca, Si and Cu via the powder mixing process route. The use of Zn, Ca, Si and Cu nano-powders in this respect and their effects on microstructure and mechanical properties of the Mg would be carried out as a part of this research. These elements chosen for this Thesis were vetted for their biocompatibility, in terms of their biotoxicity and proof of their biodegradability via literature review. The experimental scope of this Thesis has been limited to the area of the mechanical processing and development of the Mg alloys, and their subsequent mechanical and microstructural characterization. The effect of the individual alloying element on the Mg was studied via the development of binary alloys and thereafter higher order Mg alloys were developed. The results indicated the generally uniform distribution of all the alloying elements used. In particular, the uniform diffusion of Zn into the Mg matrix is observed while the extent of diffusion into the Mg particle by other elements were also observed.

Mg6Zn, Mg0.4Ca, Mg0.5Cu and Mg1Si were developed as binary alloys, of which Mg6Zn and Mg0.5Cu were of significantly high strength and ductility while the rest of the binary alloys were also of improved strength compared to unalloyed Mg. The UTS of the alloys

were found to be in the following order Mg6Zn>Mg0.5Cu>Mg0.4Ca>Mg1Si. In comparison, the UCS decreased for the Mg0.4Ca and Mg1Si as compared to unalloyed Mg while the rest showed improvement under compressive stress as well. A general decrease in ductility of the alloys occurred compared to Mg.

Higher order alloys based on the ZX system (Mg6Zn0.4Ca0.5Cu, Mg6Zn0.4Ca1Si and Mg6Zn0.4Ca0.5Cu1Si) were developed successfully with improved strength as compared to unalloyed Mg. It was found that Mg6Zn0.4Ca0.5Cu had an increased TYS and UTS compared to unalloyed Mg (92.4% and 64.7% increase respectively) with significant increase in compressive strength as well. Meanwhile, the ZX alloys containing Si were found to have the highest CYS (198.38 MPa and 192.55 for Mg6Zn0.4Ca1Si and Mg6Zn0.4Ca0.5Cu1Si respectively) and high UCS while having a modest increase in tensile strength as well i.e. a 56% and 52.7% increase in UTS for Mg6Zn0.4Ca1Si and Mg6Zn0.4Ca0.5Cu1Si respectively.

ملخص الرسالة

الاسم الكامل: مير توفيق الإسلام

عنوان الرسالة: تطوير سبائك المغنيسيوم القابلة للتحلل عن طريق القذف

التخصص: الهندسة الميكانيكية

تاريخ الدرجة العلمية: أبريل 2019

التحديات التي واجهت استخدام المغنيسيوم كمعدن قابل للتحلل الحيوي لاستخدامه في عمليات الزرع الطبية ناشئ من معدل التحلل المرتفع له وتم التغلب عليها عن طريق خلطه مع معادن أخرى.

تقوم هذه الرسالة بمهمة تطوير سبائك المغنيسيوم القابلة للتحلل الحيوي والتي تتكون من الزنك والكالسيوم والسيليكون والنحاس عن طريق عملية خلط المسحوق. في هذا الصدد سيتم استخدام مساحيق من الزنك والكالسيوم والسيليكون والنحاس ودراسة تأثيراتها على البنية الدقيقة والخواص الميكانيكية لسبيكة المغنيسيوم كجزء من هذا البحث. تم فحص هذه العناصر المختارة لهذه الرسالة للتأكد من توافقها الحيوي، من حيث السمية الحيوية وإثبات قابليتها للتحلل الحيوي من خلال مراجعة الأدبيات. يقتصر النطاق التجريبي لهذه الأطروحة على مجال المعالجة الميكانيكية لسبائك المغنيسيوم وتطويرها، وتوصيفها الميكانيكي والحيوي اللاحق. تمت دراسة تأثير اي عنصر من السبائك بشكل فردي على المغنيسيوم وذلك من خلال تطوير السبائك الثنائية ومن ثم تم تطوير سبائك المغنيسيوم ذات الرتبة العليا. أشارت النتائج بشكل عام إلى التوزيع الموحد لجميع العناصر المستخدمة في تصنيع السبيكة. لوحظ انتشار موحد من الزنك في مصفوفة المغنيسيوم على وجه الخصوص، في حين لوحظ أيضا مدى انتشار العناصر الاخرى ايضا في جسيم المغنيسيوم.

تم تطوير Mg6Zn و Mg0.4Caو Mg0.5Cuو Mg1Siكسبائك ثنائية، منها Mg6Zn و Mg0.5Cuواللتان كانتا عالية القوة والمرونة بشكل كبير بينما بقية السبائك الثنائية كانت أيضًا ذات قوة محسّنة مقارنةً بالمغنيسيوم غير المخلوط. تم العثور على قوة الشد القصوى للسبائك لتكون بالترتيب التالي:

Mg6Zn > Mg0.5Cu > Mg0.4Ca > Mg1Si، في المقابل انخفضت قوة الضغط القصوى بالنسبة إلى Mg0.4Caو Mg1Siبالمقارنة مع المغنيسيوم غير المخلوط بينما أظهرت البقية تحسنا تحت ضغط قوى الضغط كذلك .حدث انخفاض عام في ليونة السبائك مقارنة بالمغنيسيوم.

تم تطوير السبائك ذات الترتيب العالي المبنية على نظامZX (Mg6Zn0.4Ca0.5Cuو Mg6Zn0.4Ca1Si وMg6Zn0.4Ca0.5Cu1Si) بنجاح مع قوة محسّنة مقارنةً بالمغنيسيوم غير المخلوط .وقد وجد أن Mg6Zn0.4Ca0.5Cuلديه زيادة في مقاومة الشد للخضوع وقوة الشد القصوى في نهاية المطاف مقارنة مع المغنيسيوم غير المسبوك (92.4 ٪ و64.7 ٪ على التوالي) مع زيادة كبيرة في قوة الضغط كذلك. وفي الوقت نفسه، تم العثور على سبائك ZX المحتوية على السليكون بأعلى قوة إنتاجية ضاغطة (198.38 و MPa 192.55 لـMg6Zn0.4Ca1Si وMg6Zn0.4Ca0.5Cu1Si) على التوالي وقوة ضغط قصوى عالية للغاية مع زيادة متواضعة في قوة الشد وكذلك ٪56و52.7٪ زيادة في قوة الشد القصوى لـ Mg6Zn0.4Ca1Si و Mg6Zn0.4Ca0.5Cu1Siعلى التوالي.

CHAPTER 1

INTRODUCTION

Biodegradable materials for implants have been in clinical use for some time now [1]. These materials have come into prominence in lieu of non-biodegradable, permanent implants which have had temporary applications to afford the body a healing period after which the implants are no longer required. The use of permanent implants for temporary applications meant a secondary operation is carried out to remove the implant. Apart from the obvious trauma and the inconvenience suffered by the patients and their families, it also meant added medical costs and medical resources are spent in this ordeal. Not to mention the economic value of time spent by all parties involved. These permanent implants were mostly either a titanium or steel-based alloys.

Common issues of left behind permanent orthopedic implants include inflammation, infection, stress shielding and consequent bone loss. Stress shielding is due to the higher stiffness of the implants, leading to the dis-use of adjacent bones and further leading to a gradual loss of bone structure and weakening of the bones.

The solution has been the use of biodegradable materials for implants which would, as the name suggests, corrode naturally within the body, after or during affording the required time for the healing. Biodegradable materials such as biodegradable polymers (polyglycolic acid (PGA) and polylactic acid (PLA) being most common), bioceramics (Tricalcium phosphate (TCP), Hydroxyapatite (HA)) and biodegradable Mg alloys [2]

have been in increasing use for this reason. The applications included bone fixatures such as nails [3], screws [4], clips [5], wires [6] and stents [7]. Of interest has been the applications involving bones, which is where Magnesium and Mg based alloys have been researched dominantly.

Magnesium has the electron configuration of $1s^2 2s^2 2p^6 3s^2$ [8], with a hexagonal close packed (HCP) crystal structure [8]. At 1.7g/cm^3 it has the lowest density amongst all structural metals [8]. It has a Young's Modulus of approximately 45 GPa [8]. In comparison, cortical bone has a density of 1.8-2.0g/cm^3 [9] and a Young's modulus of 7-30GPa [9]. This closeness in these properties is an advantage for which Mg and its alloys have been of significant research as a biodegradable implant material.

Magnesium has been found to have special osteoconductive properties which is much appreciated when used as bone implants. It has been reported that Mg, as a cofactor of the alkaline phosphatase isozymes, helps in the healing and remodelling of the bone tissue [10].

Mg based stents are also useful where biodegradable nasal stents could help avoid treatment failure that occurs due to the secondary operations that are required of traditional implants [11].

In the dental field the use of scaffolds made of Mg/PLGA porous composites to improve bone healing following tooth extraction has been used [12]**.** And more recently, in the dental and orthopedic fields, Mg in bone cement composites have been used to obtain a high strength cement with both biodegradability and bioactivity in the form of tricalcium silicate/magnesium phosphate composite cement [13].

Still others have used Mg in magnesium/calcium phosphate cements to induce improved cellular response of bone marrow stromal cells (BMSCs) [14]. Mg ions have been known to promote osteogenic activity of bone marrow stromal cells [15]. Furthermore, various studies have been conducted to observe the effect of Mg alloys on mesenchymal stem cells [16][17].

B. Kanter et al. (2018) [18] has demonstrated the suitability of magnesium phosphate cements in partially load bearing defects of a sheep model. However, Magnesium phosphate is also one of the mineral components of kidney stones [19], although any potential relationship between that and the biodegradable Mg based cement is not clear.

The potential application of biodegradable Mg alloys is not limited to its use as temporary implants. Research has been carried out to investigate the utilization of the fast degradation characteristics of Mg with aqueous media, or in this case blood, to provide the thrust in Mg based micromotors [20]. Moreover, research into a magnesium-molybdenum trioxide based biodegradable battery has been conducted [21] to investigate the potential applications to power bioresorbable transient implants.

There has also been a number of research carried out to improve the surface properties of the traditional implants with the use of Mg to achieve better performance. These include the co-implantation of Zn/Mg ions on titanium dental implant surfaces to improve osteogenesis [22] properties of the implant, and the Mg ion implantation on micro and nano structured titanium surfaces to improve its osteogenic differentiation and proliferation of bone marrow cells [23] so as to achieve greater contact of the corroding implant and the healing bone tissue.

CHAPTER 2

LITERATURE REVIEW

2.1 Biotoxicity of the common Magnesium alloying elements.

The nutritional requirements of the human body and therefore by extension the tolerance of the body to different elements vary by ethnicity - which can be said to be differentiated by geography and culture. For instance, it has been reported by WHO [24] that there exists a wide difference of dietary intake of Ca levels between the different regions of the world, which has been attributed to the different diets based on food culture and availability. This is an indication of the differences in allowances when considering each specific group of people. Therefore, this variation in tolerance needs to be respected when choosing the Mg alloy for use as implants. The degradation rate should be within these tolerances to avoid unnecessary complications.

The nature of the chemical reaction and thereby the toxicity of the alloying elements is dependent on identifying the speciation of the elements in the extracellular fluid, which is the medium of their transport to various other locations. This is however a difficult task as the metals in the biological environment could form complexes with any of the available potential ligands and as many of the metal complexes are kinetically labile i.e. susceptible to be altered [25]. For this reason, the toxicology of the alloying elements will be discussed on the basis of their general toxicology and nutritional value rather than the specific effects

of their individual species. Moreover, for the purpose of relevancy to the topic, toxicology of the inhalation route of exposure to the metals are not discussed.

2.2 Toxicology & Pathophysiology of the common alloying elements

Mg: The human skeleton contains about 50-60% of the body's Mg, 1% in the extracellular fluid and the remaining in the muscles and tissues [24]. It is also an essential element involved in the regulation of potassium fluxes and the metabolism of Ca [24]. The Mg forms a surface constituent of the hydroxyapatite mineral component in the bone and acts in the regulation of Mg content in the serum at times of deficiency. At times of plenty in erythrocyte Mg, the bone mineral density increases and in times of deficiency, it helps make up the Mg amount to a certain extent and this form of accessible Mg availability has been reported to decrease significantly with age [24].

Fe: Iron is an essential element for the human body [26], and it is one of the most abundant metals in the body. Iron is essential for oxygen transport (Hemoglobin), and cellular functions such as synthesis of RNA and DNA, as well as synthesis of proteins and is also involved in the regulation of gene expression among many other functions [26]. Additionally, low levels of Iron in the body has also been known to cause anemia. However, an excess of iron, or an iron overload, has also been reported to lead to abnormal interference in the body and cause serious health issues leading to death if left untreated [26]. These include iron complications arising from altered iron content in cells and tissues [26].

Ca: Calcium helps provide rigidity to the human skeleton and its ions are involved in many aspects of the body's metabolism [24]. It is the 5th most abundant element in the human body and constitutes about 2% of an adult's lean body mass [24] of which, almost all are

found in the human skeletal system including the teeth and the soft tissues. About 0.1% of the total Calcium in the body is available in the extracellular fluids and are present in the form of ions (1.20mmol/l or 4.8mg/100ml) and complexes (1.6mg/100ml or 0.4mmol/l) [24]. Low levels of Ca is regulated via bone resorption and higher intake of Ca is absorbed back while the excess unabsorbed Ca is excreted out in the feces [24]. The bone mineral serves as a reservoir in this process. However, very high doses of Ca in the carbonate form have been reported to lead to precipitation of Ca salts in the renal tissue, while Ca deficiency leads to osteoporosis [24].

Zn: Zinc is an essential element with its presence in all body tissues and fluids, though the plasma zinc accounts for only about 0.1% of the total zinc content in the body. It is essential for the enzymes involved in the metabolism of nutrients such as carbohydrates, lipids, proteins as well as nucleic acids [24]. Furthermore, it is even essential for genetic expression and helps to stabilize the molecular structures of membranes and other components of the cells. Zn has a concentration presence of 0.46μmol/g (30μg/g) in the lean body mass [24]. The plasma zinc is regulated via homeostatic control.

Cu: Cu is an essential trace element [27] [28]. Cu^{2+} affects gene expression in mammals [29]. Important catalyst for synthesis of heme and absorption of iron [27]. Third most abundant trace element in the human body [27]. It is commonly obtained by the body via ingestion i.e. as water contaminants or as nutritional components of food. This pathway of absorption of Cu into the body is well regulated and most of the follow up reactions are well documented [28]. However, as a use in biodegradable material, the cellular tissues could be exposed to free Cu ions which, at concentrated levels could lead to cellular damage due to its inherent highly reactive nature. Although transmembrane transporters

and metallochaperones exist to control the levels of intra cellular copper [28], care should be taken in designing implants so as not to dissociate too much Cu into the surrounding contact fluid. Freely available Cu can be potentially toxic if it oxidizes lipids and proteins leading to the formation of intracellular and extracellular toxic free radicals [29]. Copper toxicity is rare and when it does occur, it affects primarily the liver [27]. Above 3 mg/L of whole blood concentration of Cu it is reported to lead to gastrointestinal symptoms of toxicity [27].

Si: Forrest H. Nielson (2000) has reported of the circumstantial evidence that Silicon is an essential nutrient for the human body [30]. Its deficiency has been reported to cause abnormal metabolism of connective tissue and bone in animal tests. Also, tests conducted on rats have shown that Si helps to avoid accumulation of Al in the brain - which has been connected to Alzheimer's [30]. Moreover, Si as a polymer in the form of polydimethysiloxane has been a popular breast implant material for some time now. However, though these Silicones have been thought to be biologically inert, they have caused inflammation and other complications over time [31]–[34]. On the other hand, the intravenous administration of Si nanoparticles has reportedly resulted in relative biocompatibility as far as acute toxicity was concerned, but showed granuloma formation indicating inflammation in reticulo-endothelial organs such as liver and spleen [35]. Therefore, the use of elemental Si in implants need more research and if it is included as an alloying element to Mg, it must be done cautiously.

Sn: Sn is not regarded as an essential element, although multivitamin and mineral supplements reportedly contain up to 0.01mg in a daily recommended dose [36]. Tin is mostly ingested into the body via canned food consumption, where the cans are lined with

or is made of Sn. At high dosage, Sn accumulates in the bones, liver and kidney. The bones being the primary site of deposition when Sn is injected intramuscular and during extended exposure to Sn even through other means such as ingestion [36].

Mn: Mn is an essential element for the human body which is regulated via homeostasis where excess Mn is mainly excreted via bile and feces. That portion of which forms conjugates with the bile is also ultimately excreted out mostly via feces and only a small amount is excreted through urine. It is mainly concentrated in liver, pancreas and kidney, but notably, it has its lowest concentrations in the fat and bones. The latter being of significance in the aspect of its effect in the current discussion. An Mn overload could affect the motor and cognitive abilities of the central nervous system, while prolonged Mn deficiencies have been reported to lead to greater occurrence of symptoms related to Parkinsonism. [37].

Al: Aluminum is rated as Generally Regarded As Safe (GRAS) by US FDA [25], due to which it is widely available in many of the food and medications. Previous studies have reported on the lack of proof for the Al accumulation in the brain [25]. However, it has been associated with neurotoxicity in recent years and has been reported to lead to Alzheimer's disease.

Ag: Silver is reported to be extremely toxic and is potentially fatal in the case of ingestion in the form of silver salts [38].

Li: It is a non-essential trace element. Due to it is similarity with Sodium and Potassium it can cross all biological barriers, and since it is not protein bound, it is excreted out by the kidneys and does not accumulate in the tissues too much. However, long term use of Li in

therapeutic medicine has been recorded to show toxic effects on kidney, thyroid and the Central Nervous System [39]. Taking into account the biodegradable nature of the implants, and the excretion of the Li from the body, the long-term exposure effects can be disregarded and as such Li is potentially useable as an alloying element of Mg pending further site-specific tests.

Ni: There is reportedly circumstantial evidence of Ni as an essential element [30], where it is necessary for certain activities of metabolism, and in animal studies conducted, its deficiency has been shown to show negative effects on growth, reproductive performance and the plasma glucose [30]. Ni deficiency has been also reported to affect the distribution of other essential elements in the body such as Ca, Zn and Fe. However, exposure of Ni in some of the forms other than oral administration have been reported to be a potential source of cancer in animals and humans [30]. It has been suspected of interfering in the functions of Vitamin B12 and Folic acid [30].

In: Indium is a non-essential element which produces some wide-ranging toxic effects depending on its form. The ionic Indium lead to renal failure upon its concentration in the kidney. It is mainly excreted in the urine. The colloidal form of Indium causes damage to the liver and spleen, and this form is mostly excreted via feces [40]. They are poorly absorbed when ingested, and are mostly stored in muscles, skin and bones [40].

Table 1 shows a summary of the toxicology of some of the alloying elements of Mg.

Table 1: Summary of Toxicology of the common Mg alloying elements.

ASTM Code	Chemical Symbol	Toxicology and Pathophysiology
-	Mg	Non-toxic except at high levels [24]. However, the upper limit is dependent on various factors such as gender/age/diet.
X	Ca	An essential element of the body [24]. Makes up the Human skeletal system.
C	Cu	It is an essential trace element of the body [27]. Above 3 mg/L of whole blood concentration of Cu leads to gastrointestinal symptoms of toxicity [27].
F	Fe	Essential for normal metabolism of cells [26]. Have been reported to be toxic to cells under certain conditions [29].
M	Mn	It is a trace element [41]. Mn^{2+} is the predominant form in human body [41]. Almost entirely excreted in the feces [41]. Leads to neurotoxic effects (manganism) only when exposed to inhalation [41].
Z	Zn	Zn is an an essential [24] trace element [29]. The plasma zinc is regulated via homeostatic control [24].
J	Sr	Sr is not an essential element. Strontium ranelate is used for treatment of osteoporosis [42].
L	Li	Non-Essential trace element without which the human body can lead a healthy life [43]. Long term dosage and high dosage can be toxic. Excreted almost completely via kidneys with low tissue accumulation [43].
W	Y	The compounds of Yttrium which are water insoluble are non-toxic but those which are water soluble have been reported to be mildly toxic [44]. Yttrium and its compounds have been reported to have caused liver and lung damage in animals [44].
V	Gd	Highly toxic as a free ion [44]. It is used after chelation as MRI contrast agents. The strength of the chelation determines the toxicity [44].
A	Al	Aluminum is rated as Generally Regarded As Safe (GRAS) by US FDA [25]. However concerns of its role in Alzheimer's due to its accumulation in the brain exist, although the consensus for this is disputed [45].
N	Ni	Circumstantial evidence as an essential element [30]. Potentially leads to Cancer in forms administered other than orally [30].
B	Bi	Found to be toxic in high doses [46].
Q	Ag	Silver is reported to be extremely toxic and is potentially fatal in the case of ingestion in the form of silver salts [47].
T	Sn	Not an essential element [48]. Found in cans and some vitamin supplements [48]. Relatively non-toxic (barring respiratory forms), but in chronic doses tends to accumulate in bones, kidney and liver and may cause liver and kidney problems [48].
K	Zr	Zirconia dental implants have been found to be biocompatible with good osseointegration with good soft tissue response [49]. Majority is excreted via urine while absorption is dependant on the species of Zr [50].
S	Si	Circumstantial evidence as an essential element has been reported [30]. Previously considered as biologically inert (breast implants), but exposure in severe doses and long term could lead to inflammation of liver and spleen [35].
E	Nd	Low to moderate toxicity has been observed [44].
E	La	Animal tests involving injection of La in solution form has been reported to cause low blood pressure, hyperglycaemia, hepatic alterations and degeneration of the spleen [44].
E	Ce	Experiments involving high dosage of Cerium injection in animals have led to fatal cardiovascular collapse [44].

All the alloying elements chosen for study in this thesis were confirmed to be biocompatible with suggestive biocompatibility of the degradation products as well. Additionally, the selected alloying elements were also subject to their mechanical performance in Mg alloys as reported in literature and was also further subjected to availability. With these criteria in mind, the elements of choice; Zn, Ca, Cu and Si were selected as alloying elements of Mg for the present work.

2.3 A word on the degradation of the selected alloying elements

Mg: A wide range of data are available on the corrosion characteristics of Mg due to degradation tests done on Pure Mg as a reference in virtually all the corrosion tests conducted in this field. The test results usually vary from one to the other due to the difference in testing parameters, work history and more importantly due to differences in the purity of the Mg. The duration of the test also affects the results due to the change in corrosion rate over time or otherwise known as corrosion characteristics. J. Hoffstetter et al. (2015) [51] conducted an immersion test in $NaHCO_3/CO_2$ buffered SBF and determined the degradation characteristics, based off the hydrogen evolution rates, of High Purity (HP) and Ultra High Purity (XHP) Mg and found that as-cast XHP Mg had an average degradation rate of ~10 μm/year and the HP Mg degraded at ~28 μm/year. However, after annealing, the HP Mg degraded at a much faster rate (~39 μm/year). Though these rates are deductions based on the hydrogen evolution rate this here is mentioned as a qualitative assessment. It shows that both the purity and the work history affect the degradation rates of the Mg. In direct studies involving the use of Hank's solution, corrosion rates of between 0.22 mm/year (as-rolled) to 0.36 mm/year (as-cast) have been obtained for the same duration of study (500hrs) [52].

Ca: An increase in Ca content in as-cast Mg-Ca alloys have observed to result in increased corrosion rates [53]. It has been reported by R.-C. Zeng et al. (2015) [54] that the effect of Ca on the biodegradation of binary Mg-Ca alloys is dual in nature. As a grain refiner, it decreases the corrosion rate of the alloy but at the same time, it accelerates the corrosion rate due to galvanic coupling between the Mg_2Ca phase and the α-Mg matrix. However, modifying this secondary phase has been reported to result in decreased corrosion rates compared with pure Magnesium [55].

Zn: Zn effect on Mg degradation is dual in nature. Zn added to form Mg-6Zn reduced the corrosion rate due to grain refinement leading to a more uniform corrosion surface [56]. This could also be due to the solid solution treatment and hot working done on the alloy leading to a uniform single phase. Similarly, the Mg^{2+} dissolution into Hank's solution has been reportedly been reduced in Mg6.5wt.%Zn alloy produced by mechanical milling [57]. However, tested in SBF, the addition of Zn has been reported to lead to a decreased corrosion resistance [58]. The increase in corrosion rate with increase in Zn content, as immersion tested in 3.5wt.%NaCl solution, has also been reported in literature [59]. Y. Yan et al. (2017) reported that an increase in Zn content achieved a reduction of corrosion potential albeit an increased corrosion current owing to microgalvanic corrosion resulting from increased sizes of Mg-Zn intermetallics [60]. So the overall effect of Zn on Mg corrosion would depend on the work history and the design of the implant in addition to the specific environment it is exposed to.

Cu: Addition of Cu to Mg results in increased degradation rates, which increases along with the Cu content [61]**.** This has been attributed to the presence of Mg_2Cu precipitates acting as the cathode in the galvanic couple formed between the Mg matrix and the

secondary phase. Binary Mg-Cu alloys have shown to increase pH in in-vitro studies, which is expected to inhibit bacterial growth. Though in-vivo, it is thought that the homeostatic regulation of the pH would take place at the site of implant.

Si: Si has been reported to decrease the corrosion potential of binary Mg1Si alloy compared to unalloyed Mg [52]. Although corrosion rate of as-cast alloy increased significantly, after rolling it achieved lower corrosion rates than unalloyed Mg. This change in corrosion rate after working could be as a result of the modification of the secondary phase Mg_2Si which is formed when alloyed with Mg [62], the presence of which provides cathodic corrosion initiation sites [63].

These findings demonstrate that Zn, Ca, Cu and Si does indeed corrode in use as an alloying element of Mg and that the processing route of the alloy and its work history affects the degradation rate.

2.4 Effect of the alloying elements on the microstructure and mechanical properties of the Mg alloy

The microstructures of Mg-alloys are mainly composed of an α-Mg matrix with some amount of alloying element in them, followed by secondary phases. These secondary phases are primarily located in the grain boundaries. The mode of formation when casting is that the secondary phases accumulate in advance of the forming grains. The secondary phases appear as precipitates along the grain boundary [64]. However, in some cases, the secondary phases are also present as dendritic structures, if present [65].

Mg: Mg in its pure form exists in α-Mg phase. Addition of further alloying elements render the different characteristics associated with the formation of their respective secondary and

tertiary phases. These initially formed phases undergo additional changes during further processing of the Mg alloy. Therefore, it is necessary to look at some of the alloying elements and the commonly formed phases with Mg, found in the literature. For this purpose, only the selected elements of choice with sufficient biocompatibility have been chosen for further discussion. Pure Mg has a UCS of about 185.67 MPa and a UTS of approximately 63 MPa [61]. The α-Mg have been reported to exist as HCP structures with dimensions of a=0.32nm and c=10.3nm [64].

Zn: Zinc forms the intermetallic phase MgZn, which is mainly present in the grain boundary [66]. It has a solubility limit of about 2.6 wt.% in Mg [67].

It has been reported by C.J. Boehlert and K. Knittel (2006) [68] that Zn of 4 wt% produced the most refinement of grain size in Mg binary alloy. Similarly S. Cai et al. (2012) [66] that addition of Zn up to 5 %wt. increased the mechanical properties of Mg alloys, which has been attributed to the grain refinement, solid solution strengthening and second phase strengthening. On the other hand, the elongation was the highest when 1 %wt. Zn was used [66].

Mg-Zn alloy produced from powder metallurgy produced fine, equiaxed grains and row elongated grains. Strike-like coarse intermetallic phases were also reportedly produced with increased Zn concentration [60].

Zn addition to Mg-6wt.%Sn was investigated by N. El Mahallawy et al. (2017) [69] with addition of Zn wt.% of 2 and 4. In as-cast alloys, Zn acted as a grain refiner to the Sn, further complimenting the grain refining characteristic of Sn itself. Addition of Zn decreased the grain size of as-rolled and as-extruded alloys as well.

Ca: Y. C. Lee et al. (2000) [70] reported that addition of Ca up to 0.4 wt% resulted in significant grain refinement of about 270 μm, and any additional grain refinement was reported to have only minor changes in grain size. Research conducted by Z. Li et al. (2008) [71] on Mg-Ca binary alloys with Ca wt% 1-3 found that the Yield Strength, Ultimate Tensile Strength and Elongation of the binary Mg alloy decreased with increasing Ca content for the as-cast alloys. The UTS and elongation were successively increased after hot rolling and hot extrusion [71]. The loss in mechanical properties have been attributed to the embrittlement of the alloy owing to the secondary phase Mg_2Ca. An increase in this Mg_2Ca was found to enhance the corrosion rate of the alloy. Formation of Mg_2Ca phase, in proximity with Fe and Si have been reported to lead to pitting corrosion [54].

Meanwhile, H.R.B. Rad et al. (2012) reported that with increasing Ca content from 0.5 wt.% to 10 wt.% significantly increased the hardness of binary Mg-Ca alloys [72]. Mg-0.79Ca with its high hardness, UTS, YS, and corrosion resistance was found to be the most promising Mg-Ca composition for use as a biodegradable material by R.-C. Zeng et al. (2015) [54]. In the presence of Si, CaMgSi phase is present in higher order alloys [73].

Cu: Recent works by C. Liu et al. (2016) produced Mg-Cu alloys of approximate grain size 100μm [61]. Mg_2Cu secondary phase precipitates form with increasing Cu content (0.05, 0.1, 0.5 wt %.) and have been reported to be present as a discontinuous distribution along the grain boundaries as well as in the grains as particles [61]. A similar study by Y. Li et al. (2016) [74] in their supplementary data reported obtaining Mg-Cu alloy grain size of about 300μm, and with increasing Cu content (0.05, 0.1, 0.25 wt%.) the presence of secondary phase Mg_2Cu becomes more visible in the form of a globular presence mainly in the grain boundaries and a small amount inside the grains.

The presence of the secondary phase Mg_2Cu has also been credited with better mechanical properties of the Mg-Cu alloys compared with pure Mg [61]. Mg-0.03Cu has been reported to have a UCS of 199.67 MPa and a UTS of approximately 83 MPa, with these values decreasing with the increase in Cu content [61].

Cu has also been added to Mg-Zn alloys to enhance the mechanical properties which gives rise to the intermetallic phases of Mg(Zn,Cu) and $Mg(Zn,Cu)_2$ [75]. M. Lotfpour et al. (2016) has reported that when added to Mg-2wt%Zn, there is an increase in mechanical properties of UTS and ductility until about 0.5wt% Cu, after which it decreases drastically, even well below that of the original alloy [75]. This behavior has been attributed to the embrittlement of the alloy due to increase in cleavage planes resulting in brittle fracture [75].

Si: Si is also a grain refiner of Mg [70]. Si has been reported to have produced about 240μm. Si forms the secondary phase of Mg_2Si, which, after annealing becomes finer and more homogenized [73]. If the Si concentration becomes more than the eutectic concentration limits, that secondary phase crystallizes in the form of needles, resulting in an increased brittleness [76]. Si, when added to Mg alloys containing Ca forms CaMgSi [73].

From the above discussion, it can be summarized that the chosen elements; Zn, Ca, Cu and Si imparts good microstructural and mechanical properties to Mg.

2.5 Common processing routes of Mg alloys

Casting is the most common method of Mg alloy development found in the literature. This usually involves the melting of master alloy ingots of Mg and alloying material in a desired proportion and recasting to obtain the desired magnesium alloy.

The casting method used also affects the properties of the alloys used. For example, J. Zheng et al. [77] studied the microstructure and mechanical properties of Mg-3Sm-0.5Zn-0.4Zr (all in wt.%) developed using both die casting and ingot casting and found that though the ingot cast alloy resulted in higher tensile strength at high temperature (200°C), that of the die cast had better tensile strength at room temperature.

Others have changed the solidification process after melting to change the properties of the Mg materials produced. These include processes such as sub-rapid solidification [78], Rapid Solidification (RS) [79] or High Shear Solidification (HSS) [80].

The conventionally developed alloys have been post-processed in a number of ways to achieve further improvement in their properties. These include the heat treatment processes such as aging, solid solution heat treatment [81] or plastic deformation processes such as rolling and extrusion [82]. P. Poddar et al. [83] produced a number of Mg alloys by gravity-die-casting and have reported on the improvement in the tensile properties of cast alloys after aging.

All these processing routes and post-development processes of the Mg are carried out to affect the final properties of the alloys/composites of Mg through affecting the microstructure of the materials. With a particular composition of the Mg alloy/composite, the single most aspect of the material that has been sought to be altered via the secondary

processes has been the distribution of the alloying/reinforcing element within the Mg matrix.

In a study conducted by N. El Mahallawy et al. [69] on cast Mg-6Sn-xZn alloys (x: 0,2,4 wt.%), it was determined that grain sizes were vastly refined after extrusion and after rolling when compared with as-cast alloy. Furthermore, the results of mechanical testing determined that the highest YS and UTS were produced for extruded alloys, followed by rolled alloys, each of the processes producing superior strength for all values of Zn [69]. The extrusion and rolling carried out post alloy production here means that the alloys were underwent plastic deformation.

J. Su et al. (2015) [84] reported that a higher rolling speed (1000m/min) achieved better rollability and weaker texture of the AZ31 alloys compared the slower speed of 15m/min. These results have been attributed to the dynamic recrystallization (DRX) taking place owing to the increased temperature of the alloy and activation of a larger number of twinning and slip systems – in particular the <c+a> pyramidal slip system. This DRX taking place is of interest since it results in more equiaxed grains and thereby increasing possible isotropy.

2.6 Powder metallurgy process route

In recent years, the Powder Metallurgy process route has been used by a number of researchers [85][86][87][88][89][90][91] to produce Mg alloys. While some studies used the atomization process on the alloyed melt [85][86][89][90][91], others have mechanically milled elemental powders [88] and still others have used the elemental powders without the mechanical milling [87] to proceed with the Blend-Press-Sinter (BPS)

process route. These processes are usually followed by extrusion of the sintered material to form the final alloy. PM has the advantage of uniform dispersal of the elements, and thereby the uniformity of the secondary phases and a greater dissolution of the alloy elements in the αMg matrix.

J. Kubásek et al. (2017) [86] reported on the superior properties of TYS and hardness of the WE43 (Mg-4Y-3RE-Zr) alloy produced via extrusion of alloy prepared by powder metallurgy when compared with that of the extruded alloy prepared using casting. In particular, the effects of solid solution strengthening and precipitate strengthening achieved as a result of the more uniform distribution of elements via the PM method has been noted. The ability to produce a uniform distribution of the secondary phases has also been reported by M. Rashad et al. (2015) [87] using conventional PM route followed by hot extrusion. Grain size refinement of as much as 500nm has been reported for Mg-6Zn-5Ca produced via PM [89].

Extrusion of Mg alloys is one of the most common mechanical processes carried out on the alloys for altering their microstructure. Researchers have used both direct extrusion process [92][93] and indirect extrusion process [94][95][96] to process the Mg alloys. Extrusion has the advantage of grain refinement of the Mg alloy via plastic deformation (with the dynamic recrystallization) and in case of the alloy being produced via the Powder Metallurgy route, it also offers the advantage of increasing the bonding between the sinter bonded particles i.e. decrease the porosity of the alloy.

Y. Yan et al (2017) conducted extrusion on a powder metallurgy sintered Mg alloy and reported that the compressive strengths of as-extruded alloys were much higher than that

of natural bone and had elastic moduli close to that of bone [7]. The produced alloys of Mg-Zn, after extrusion, had fine equiaxed grains and row elongated grains [7].

Mg alloys produced via powder metallurgy has also been reported to have produced greater corrosion resistance - attributed to the grain refinement and the homogenized microstructure [24][25]. The superiority of powder metallurgy in grain refinement and/or homogenization of the microstructure as compared to a WE43 Mg alloy produced from casting has also been reported by J. Kubasek et al. (2017) [23].

Moreover, H. Asgharzadeh et al. (2014) [26], investigating Mg-Zn-Y alloys produced via powder metallurgy, has reported that using smaller nano sized particles resulted in a finer and more homogeneous microstructure with improved mechanical properties.

Literature survey has revealed that only a few studies have been carried out to investigate the effects of Zn and Ca on magnesium through the powder mixing process route. Especially the use of nano particles of Zn, Ca, Si and Ci in this regard have not been found. This is also the case for the Mg-Zn-Ca alloy system. Therefore, the effects of the use of these nano particles on the properties of Mg produced from powder mixing process, be it individually or in combined form as Mg-Zn-Ca system, is to be studied. It is expected to yield more uniform distribution of secondary phases than obtained via casting and is also expected to achieve grain refinement.

2.7 Blend-Press-Sinter process route

Despite the advantages of PM, it has been reported to lead to difficulties in controlling the micro-alloying and the cold-weld formations. To overcome this issue a number of attempts have been made by researchers to utilize the Blend-Press-Sinter (BPS) processing route.

In recent years a number of studies have been carried out using the BPS+E (BPS followed by Extrusion) process to develop Mg materials though most of the concentration has been on Mg composites a few has also been on the development of Mg alloys.

2.7.1 The case for the use of Extrusion process and for the use of nano particles

Previous work on Mg composites using the BPS process route followed by extrusion produced [97]. Mg composites with Ni reinforcement particles were developed using the BPS + Extrusion process route and was reportedly achieved reasonably uniform distribution of Ni particles in the Mg matrix [97].

Work carried out to study the effect of sintering method on the final properties of the Mg composite containing nano-Y_2O_3 particles found out that an increased ductility and work of fracture was produced in conventional slow heating method compared to microwave assisted sintered composites [98].

2.8 The selection of the weight content of the chosen alloying elements

The weight content of the alloying elements were chosen keeping in mind the reportedly good properties of the Zinc-Calcium (ZX) system of Mg alloys. Since there is reportedly good mechanical properties of the ZX system and the reportedly good diffusion characteristics of Zn into the Mg particle achieved by Fida et al. [99], a 6 wt.% Zn is chosen for the Zn. On the other hand, the main benefit of the ZX system in biodegradable implants is the presence of Ca, the 0.4 wt.% of Ca chosen as the Ca content fraction reportedly produced highest grain refinement and any further addition resulted in only negligible grain refinement [70].

Si was chosen as a study element to determine its effect, so for the purpose of comparison, 1 wt.% Si was chosen, similar to that produced by casting in [52].In the case of Copper, 0.5 wt.% Cu was chosen as an arbitrary content to study the effect of Cu on Mg.

2.9 Summary

Extensive literature review suggests that the use of BPS+Extrusion (BPS+E) process route for development of Mg alloys is limited. BPS+E has been used mainly for the development of Mg composites in the past. BPS has been used for the study of an MgZn alloy developed via microalloying recently.

A study of binary alloys of Zn, Ca, Cu and Si developed via the BPS+E processing route using nano powders of these alloying elements have not been found in research and as such this current work will serve to understand the effect of these elements on Mg produced using this processing route.

Furthermore, the literature review of Mg alloys does show that a Zn and Ca based system of Mg alloys produced mainly by casting techniques have been of interest for their good biocompatibility and performance. However, incorporation of the MgZnCa system of alloys with Cu and/or Si has not been shown, especially the compositional variety produced by BPS+E processing route using nano powders is perhaps the first of its kind to be attempted.

Therefore, it is to be stated that the objective of this thesis is to study the effects of Zn, Ca, Si and Cu on the Mg when used as alloying elements in nanosized powder form via the development of binary alloys of Mg using the Blend-Press-Sinter process route followed by hot extrusion, and the development of higher order Mg alloys based on the MgZnCa. The scope of this thesis is the physical development of the alloys and their microstructural and mechanical characterization.

CHAPTER 3

MATERIALS & EXPERIMENTAL PROCEDURE

The Mg alloys were formed via conventional BPS (Blend, Press, Sintering) process route followed by extrusion, using powders as the raw material. Described below is the process along with the process parameters.

3.1 Process methodology

The alloys are to be developed using the powder mixing processing followed by hot extrusion. This process involves obtaining the powder samples as a pre-determined weighed fraction and mixing the powders to obtain a homogenous mixture which is then compacted/consolidated using a press machine to produce the green billet. The green billet is then sintered to obtain the final alloy which is then further hot extruded to obtain the required study samples.

Figure 1: Block diagram of the process using powder mixing followed by extrusion.

3.1.1 Starting Materials

The starting materials are powder obtained commercially. The Magnesium powder, manufactured by Merck KGaA, Germany, was of purity >98.5% and consisted of particles of average size 60-300 μm. The Calcium powders were of >99.8% purity and average size

of 80-100 nm particles from Nanoshel LLC, USA. Zinc powders were of size 80-100 nm with 99.9% purity from Skyspring Nanomaterials Inc., USA.

Copper powders of 99.8% purity and average particle size of 25 nm according to commercial label were also obtained from Skyspring Nanomaterials Inc., USA. The Silicon was also used in the powder form, with >98% purity and 100 nm average particle size from Skyspring Nanomaterials Inc., USA. XRD analyses of the powders and the FESEM images of the powders are given below in Figure 2 and Figure 3 respectively.

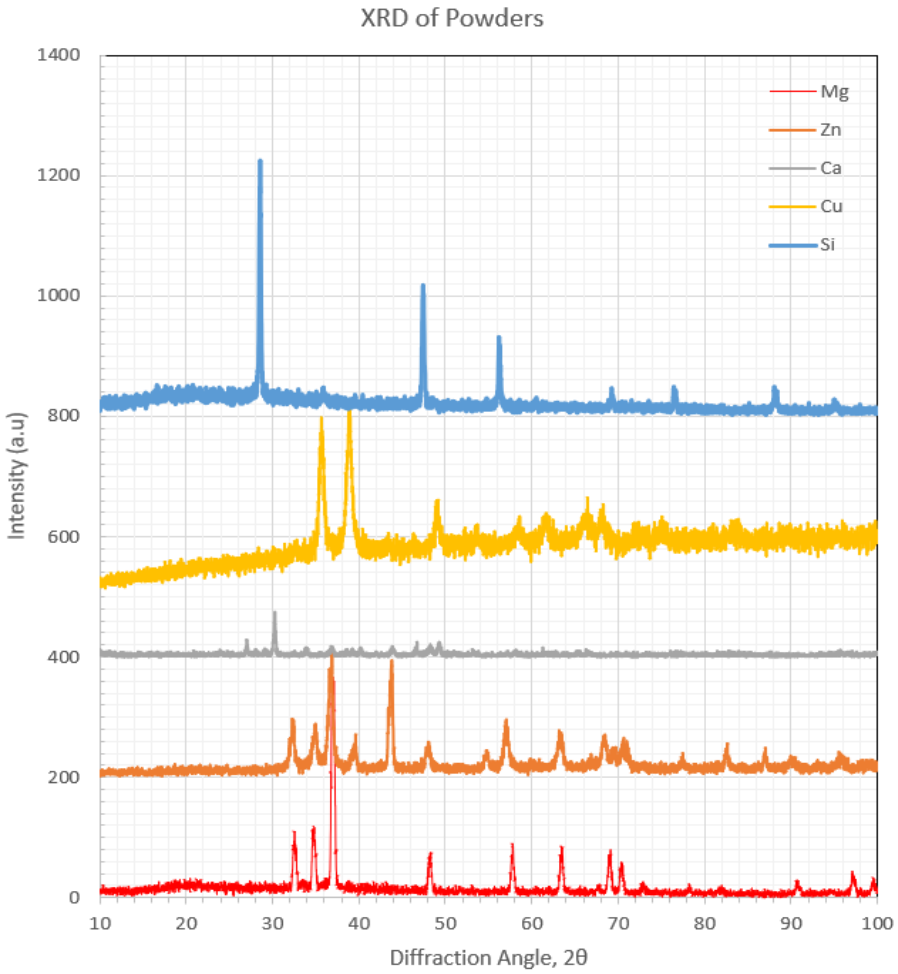

Figure 2: XRD results of the elemental powders.

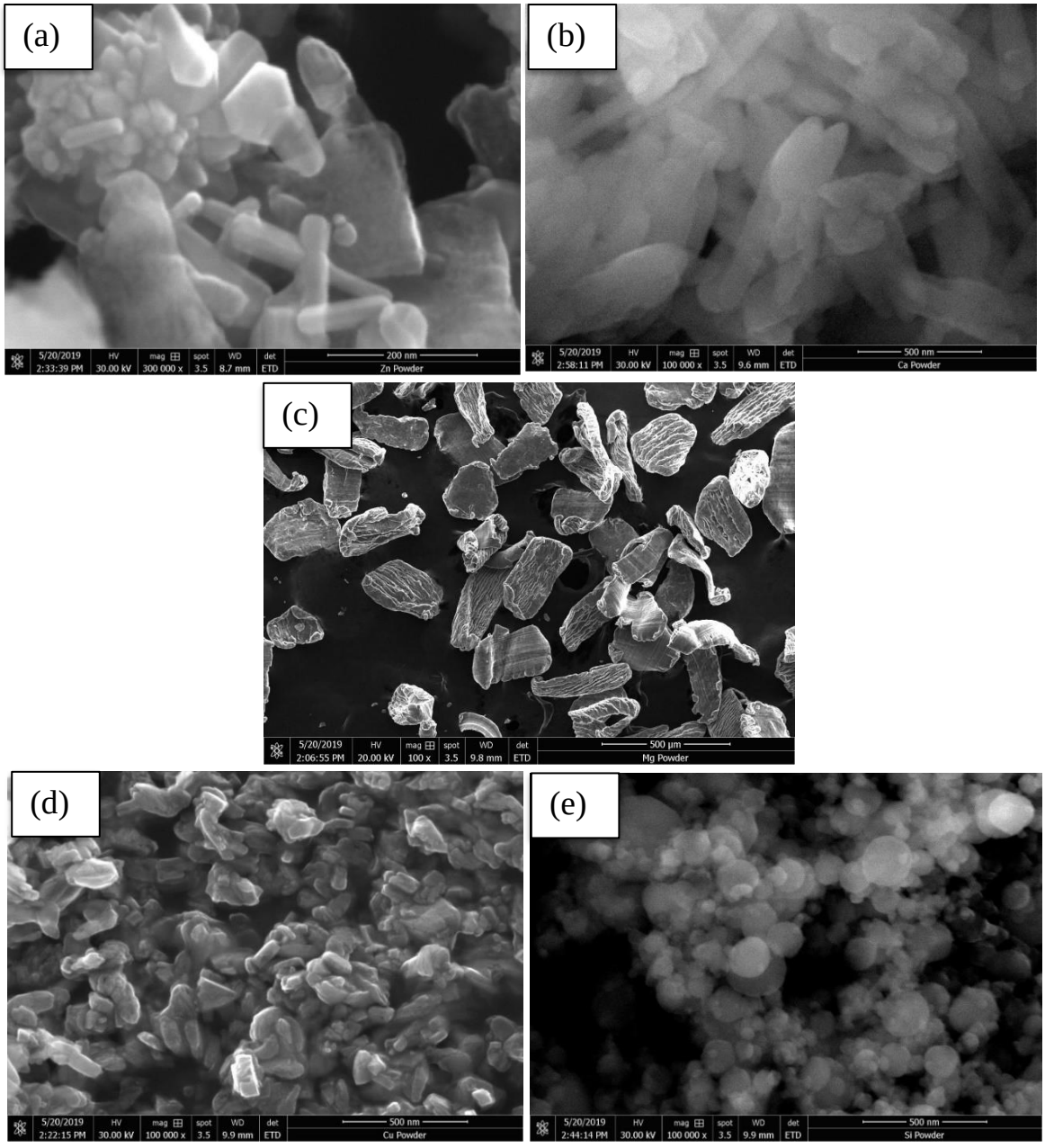

Figure 3: FESEM images of powders of (a) Zn, (b) Ca, (c) Mg, (d) Cu and (e) Si.

3.1.2 Powder mixing/ Blending

The powders were weighed proportionately for a green billet of 35mm dia and height of 40mm. The proportions were based on weight fractions of the final billet rather than the volume fraction. It was then mixed using a planetary ball mill (Fritsch Pulverisette 5) without the use of balls to achieve a homogenous and uniform distribution of the alloying elements in the bulk of Mg particles. They were mixed at a speed of 200 rpm for one hour.

These parameters are chosen based on literature involving similarly produced Mg composites [97][100] and Mg alloy [99] which reportedly produced good uniform distribution of the powders.

3.1.3 Powder Compaction

The blended powders were poured into the compaction die cavity and pressed using a uniaxial hydraulic press of maximum capacity 150-ton force (Figure 5). Colloidal graphite in spray form was applied to the contacting surfaces prior to the powder being transferred to the die. A compaction pressure of 450 MPa was applied for 2 minutes and then released to form the green billet. Similar studies found in literature have reported compression pressures of although the holding time have been reported to be either 1 [97] or 2 mins. The process is as shown in Figure 4.

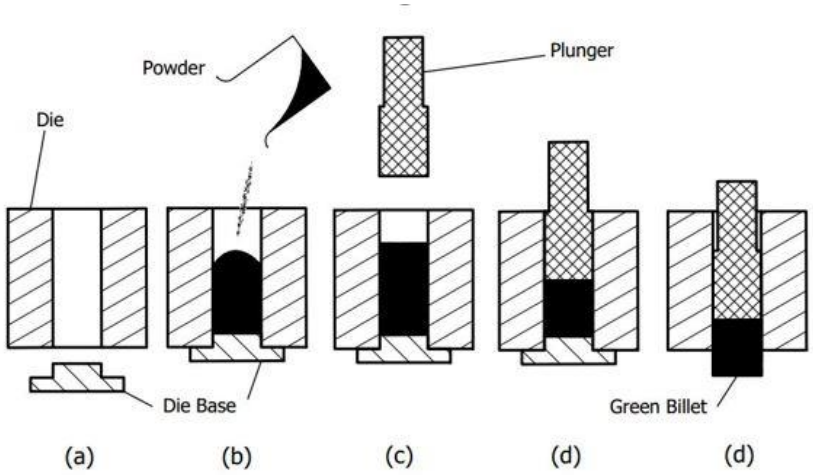

Figure 4: Schematic diagram of the compaction process carried out.

Figure 5: Uniaxial hydraulic Press used for Compaction and Extrusion.

3.1.4 Sintering

The green billets were sintered in a tube furnace (MTI GSL-1700X, MTI corporation, USA) under Argon gas. Two different heating regimes were used for sintering; those

without Zinc were held at 500 °C for two hours while those with Zinc were first held at 400 °C for an hour before proceeding to the 500 °C stage where it was held for another 2 hours before being furnace cooled. Previous studies have reported excellent results with these parameters for sintering similarly produced Mg materials [101][99][97].

In both cases the heating rate was set at 10 °C/min and all samples were furnace cooled at the end of their sintering regimes. The extra caution was taken for Zn containing samples in order to allow it to form intermetallics and avoid melting directly [99].

Figure 6: Tubular furnace used for sintering of the Green billet.

3.1.5 Extrusion

The sintered samples were then uniaxially extruded using a hydraulic press of 150 tonne capacity (Figure 5). The extrusion ratio was 19.14:1 to obtain rods of 8mm diameter. This particular extrusion ratios have been found to have resulted in defect free Mg composite rods [97]. The extrusion die setup was separately heated to the extrusion temperature while the sintered samples were heated a little above extrusion temperature to take into account the heat loss in handling. Extrusion was carried out at temperatures of 300 °C while those containing Zinc were extruded at 350 °C. Prior to extrusion, the samples were heated in a furnace for 2 hours at 350 °C while similarly those with Zinc content were heated at 400 °C. Colloidal graphite was applied in spray form to the contact surfaces of the extrusion to minimize friction.

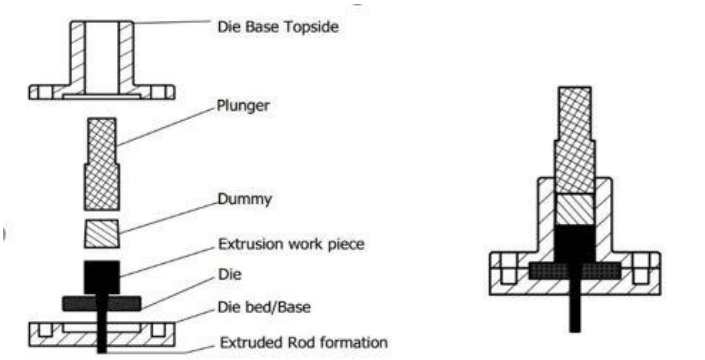

Figure 7: Schematic diagram of the extrusion setup - exploded view on left.

3.1.6 Sectioning

Rods of ~8.4 mm dia were obtained after extrusion. The samples for the preceding experiments were taken from these rods. Specifically, tensile samples were machined to the dimensions discussed in the relevant section below and the samples for compression testing, XRD testing, metallography, hardness testing, density and SEM analysis were all

cut using either a Dremel rotary tool or using a hand saw to the appropriate sections followed by appropriate grinding and polishing.

3.2 Analysis methodology

The analysis of the samples was done taking the defect-free samples sectioned from the Mg-Alloy rods. This meant not taking samples from the very beginning of the sample to avoid any concern of misrepresentation of the main rod alloy. Care was also taken to avoid the use of center hollow defective samples which sometimes did come up towards the end of the extruded rods. Further cautions taken during each test is discussed in the relevant sections below.

3.2.1 Density measurement

Cut sections of the samples for the compression testing were used to obtain density measurements for the Mg alloys. Density was measured using the Archimedes Principal [102] by immersing the samples in a water bath and comparing with the dry weight of the samples as follows:

The density was measured using 3 randomly selected cylindrical samples with surfaces smooth to 1200 grit size to avoid bubble getting caught in any rough edges. The samples were weighed in an electronic balance (Mettler Toledo model AG285) with an accuracy level of ±0.0001 gm. Immersion fluid in this purpose used was distilled water.

$$\rho_{alloy} = \left(\frac{Weight\ of\ alloy_{\ in\ air}}{Weight\ of\ alloy_{\ in\ water}}\right) * (\rho_{water} - \rho_{air}) + \rho_{air} \quad \textbf{(1)}$$

The experimental densities were compared with the theoretical density of the Alloys.

The theoretical density of the alloys were obtained using the equation below [8]:

$$C_1 = \frac{m_1}{m_1+m_2} * 100 \quad \textbf{(2)}$$

Where C_1 and C_2 are the concentration of the elements 1 and 2 in wt.% and m_1 and m_2 are their corresponding weights, and so to obtain the average density of the alloy, ρ_{av}, use the equation below [8]:

$$\rho_{av} = \frac{100}{\frac{C_1}{\rho_1} + \frac{C_2}{\rho_2}} \quad (\textbf{3})$$

Therefore, % porosity is simply as follows:

$$\%\ \text{porosity} = \frac{\rho_{av} - \rho_{alloy}}{\rho_{av}} \quad \textbf{(4)}$$

3.2.2 XRD Analysis

XRD analysis for all the specimens were carried out for the alloy cross-sections using Bruker-AXS D8 Advance -40kv/40 Ma. A step size of 0.02 deg for an angle range of 10-100 degrees were carried out using Cu-Kα radiation.

3.2.3 Microstructural characterization

Microstructural characterization was done using optical microscope (Nikon and DSX-510, Olympus, Japan) and a Field Emission Scanning Electron Microscope (FESEM) (Quanta, 250 FEG, FEI, Czech Republic) with an Energy Dispersive Spectroscopy (EDS) mounted on it.

Surface images of the polished alloys were taken using Secondary Electron Imaging (SEI) and the etched micrography was done using the optical microscope. Both the compressive and tensile fractography was also analyzed using the FE-SEM to determine the fracture mode.

3.2.3.1 Grain Size measurements

Sectioned extruded rod samples were prepared for etching by grinding it to a finished grit of 1200 followed by polishing with Alumina powder (0.05μm) on a polishing cloth wetted with water. The samples were then etched using acetic picral solution and optical micrographs were taken to observe the grain boundaries and grains.

A Matlab program (LINECUT) was then utilized to obtain grain sizes from the calibrated Mg alloy optical micrographs via the method of counting and measuring the grain sizes intersecting a grid of horizontal lines.

3.2.4 Mechanical characterization

3.2.4.1 Hardness

The macro hardness test was done using the Rockwell superficial scale of HR15T using a hardened steel ball of 1/16" dia. Care was taken to avoid the edges of the sectioned alloy, keeping a distance of about 2.5 indentation dia from the edge. Similar distance was kept to avoid any effects of strain hardening in the final reading.

The micro hardness tests were done using Vickers Hardness testing machine with a load of 50 g_f and a dwell time of 15 seconds. Between 10-16 readings were taken for each alloy. Where the particle boundaries are visible, specific readings were also taken from the particle boundaries.

3.2.4.2 Tensile Test

The tensile tests were performed according to the ASTM E8/E8M-16a using an Instron 3367 machine (Instron, USA). Figure 8 shows the specimen dimensions to which the tensile samples were machined. Equations 5-7 show how the stress, strain and work of

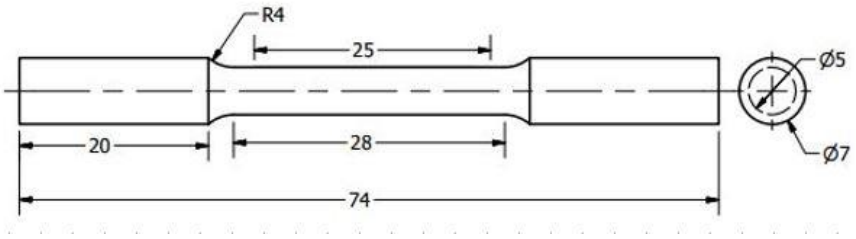

Figure 8: Tensile Test Specimen machining dimensions.

fracture was calculated. The work of fracture was calculated as the area under the stress-strain curve. The yield strength was determined using the construction of a line parallel to the initial slope of the stress-strain curve and offset by 0.2% of strain.

$$Stress\ (\sigma) = \frac{Tensile\ Force}{Original\ Area} \quad \textbf{5}$$

$$Strain\ (\varepsilon) = \frac{Extension}{Original\ Length} \quad \textbf{6}$$

$$Work\ of\ Fracture = \sum_{i=2}^{N} \left\{ \frac{1}{2} (\varepsilon_i - \varepsilon_{i-1})(\sigma_i + \sigma_{i-1}) \right\} \quad \textbf{7}$$

3.2.4.3 Compressive Test

The compressive tests were also done on an Instron 3367 machine (Instron, USA) using samples of L/D ratio 1-1.2. The samples were ground and polished to a near perfect cylinder with error of 0.02 - 0.05 mm from circular surface to surface. The stress, strain, work of fracture and the yielding point of the samples were calculated in a similar manner as the tensile tests.

3.2.5 Fractography

The fractured tensile samples of the respective Mg alloys were observed under high magnification to study the fractographic characteristic of the alloys under the axial overload condition. Field emission scanning electron microscope (FESEM) (Quanta 250 FEG, FEI, Czech Republic) was used for the fractography. The fractography samples were kept in air tight condition in sealed bags to avoid contamination and oxidation of the fractured surface.

CHAPTER 4

RESULTS AND DISCUSSION

4.1 Procedure and methodology

There were no observed macro-defects such as cracking on the compressed billet as well as the sintered product. The extruded rod did not show any longitudinal or radial cracks or any signs of orange peeling. Similarly, for the most part ends of the rod did not have any piping phenomena observed. The little which was observed can be attributed to experimental setup deficiencies leading to discontinuity of the heating of the extrusion bed while extruding. This can be corrected by a continuous heating setup. Apart from that, the near perfect densities of the alloys obtained indicate the suitability of the development process and parameters.

Table 2: Density and porosity results.

Material	**Actual Density, g/cm^3**	**Theoretical Density, g/cm^3**	**Porosity, %**
Unalloyed Mg	1.719	1.740	1.230
Mg6Zn	1.820	1.823	0.172
Mg0.4Ca	1.738	1.739	0.072
Mg0.5Cu	1.746	1.749	0.176
Mg1Si	1.735	1.744	0.522
Mg6Zn0.4Ca0.5Cu	1.817	1.829	0.700
Mg6Zn0.4Ca1Si	1.820	1.827	0.345
Mg6Zn0.4Ca0.5Cu1Si	1.829	1.834	0.278

The blending of the powders is expected to have resulted in a uniform coating of the larger Mg particles with the nano sized alloying element powders as was reported [99]. The

densification of the alloy begins with the compaction of the blended element powders. The individual powders are cold compacted until the particles become closer and the gap between them is decreased. At this point, the presence of cold weld formation between the Mg particles, assisted by the alloying elements present between the particles is expected to bond the Mg particles and result in the green billet. This green billet is very porous and is then sintered to a final temperature of 500°C. The increase in temperature is expected to cause solid state diffusion of the alloying elements into the Mg particles and/or alloy with each other and/or Mg to form intermetallic phases. This process increases the bonding between the particles and decreases the porosity between them. For the alloys containing Zn, the Zn is expected to melt at around 419.5°C and the extra sintering step at 400°C is therefore done to encourage the Zn to also undergo the solid-solid diffusion and/or form intermetallic phases.

The extrusion of the sintered sample is then extruded at a very high extrusion ratio (19.4:1) and at a temperature of 250°C/300°C. This temperature is well above the dynamic recrystallization temperature of Mg and therefore the extensive plastic deformation that the alloy undergoes while being extruded is expected to further reduce any pores present inside it to a minimum. The presence of pores as trapped air or formation of pores due to mismatch between the thermal expansion co-efficient of the different particles involved could also give rise to some porosity of the end-product. An actual density of the alloy close to the theoretical density of the alloy indicates minimal porosity and is validation of the suitability of the process and the process parameters employed.

Aside from the densification, it has to be noted that the alloys were extruded at two different temperatures. The extrusion was started with the unalloyed Mg and binary alloys except

for Zn, and was carried out successfully at 250°C. However, the binary alloy containing Zn was not extrudable at that temperature. Thereby the temperature was raised to 300°C and it was found to be compatible. Further alloys based on the Zn system was therefore carried out at 300°C. An additional unalloyed Mg was also extruded at 300°C to serve as a suitable reference for the 300°C extruded alloys. The unalloyed Mg extruded at two different temperatures (250°C and 300°C) were labelled as Mg250 and Mg300 in the discussion henceforth.

4.2 Effect of the Alloying element on Mg

4.2.1 A brief discussion on the unalloyed Mg:

Before delving into the effect of the alloying elements, a brief discussion on the results of the microstructure of the unalloyed Mg is presented here to better understand the governing mechanisms.

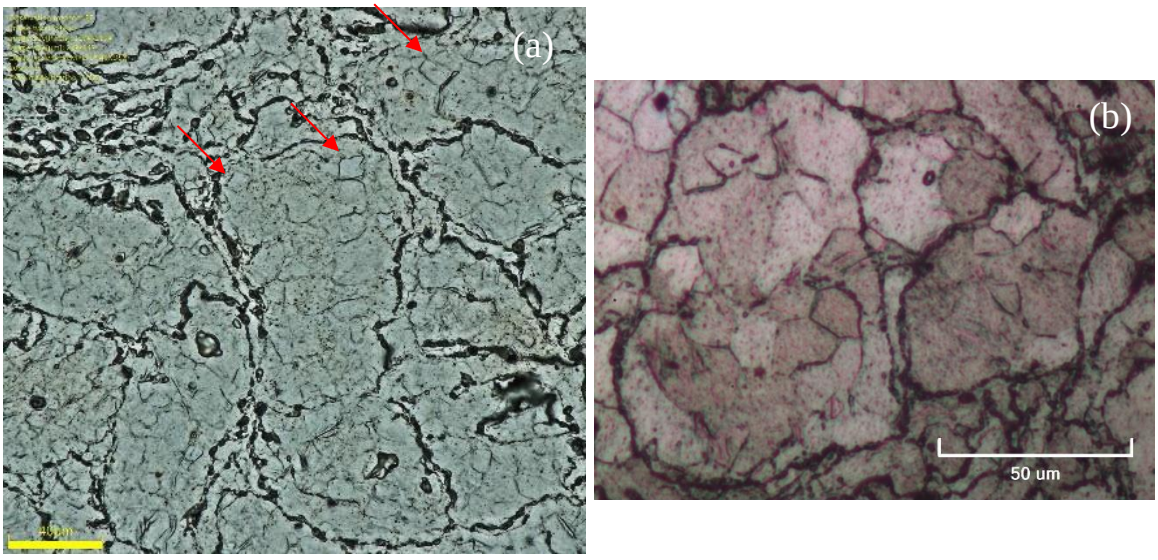

Figure 9: Etched optical micrograph of unalloyed Mg (a) sintered at 300°C and (b) that which was sintered at 250°C.

It has been reported that at room temperature, the plastic deformation of Mg forms high density dislocation pile-ups within the grains resulting from extensive twinning [103]. The recrystallization of the grains occurs at the twins during deformation, and

Between 150°C-300°C temperature range, increasing the temperature has been reported to lead to increased frequency of TRDX (twinning recrystallization) and an increased volume fraction of grains are recrystallized [103]. Therefore, Mg300 is expected to have undergone more of TRDX and have more recrystallization taken place than Mg250. This could explain the wider spectrum of grain sizes in Mg300 compared to Mg250.

The etched optical micrograph of the extruded unalloyed Mg, sintered at 300°C, shows the grain sizes between 2.5-23.9μm with a mean of 9.6μm. However, these grains were near equiaxed. Since the extrusion temperature was well above the DRX temperature of Mg the equiaxed grains could indicate the occurrence of DRX during the extrusion process. This wide range in grain sizes could be a result of presence of impurities (Figure 10) and oxides, especially around the periphery of the Mg powders.

The difference between the two Mg were examined and found to be slight in terms of microhardness (Figure 11), TYS and UTS (Figure 13) but differ in tensile ductility. They also have differences in grain sizes (Figure 10) and compressive properties (Figure 12).

The increased compressive strength and the increased ductility could be explained by the slightly lower average grain sizes of the Mg300 compared to Mg250.

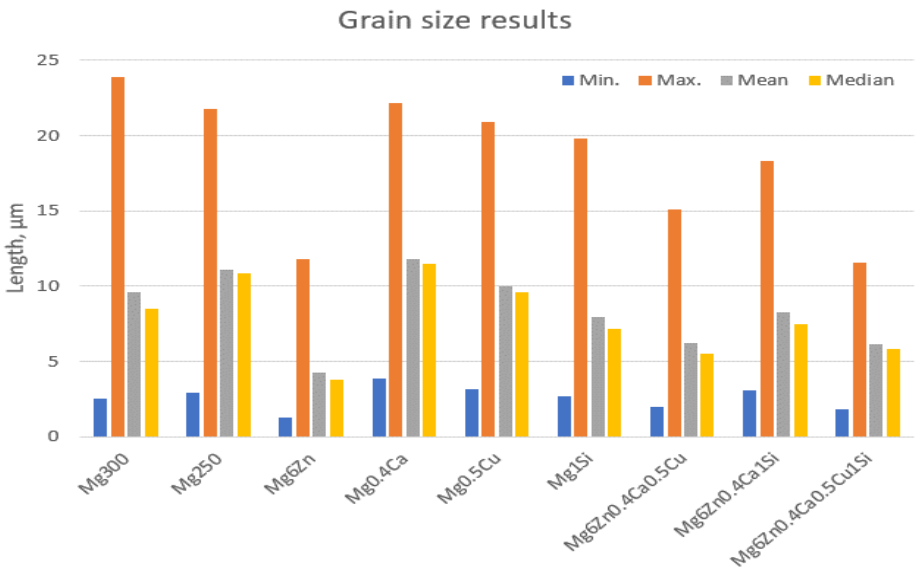

Figure 10: Summary of Grain size results (as obtained from LINECUT-Matlab program).

The no change observed in tensile strength and the improvement in compressive strength of the Mg300 compared with Mg250 could perhaps be that Mg300 benefits from the wider range of grain sizes in it. It is not hard to imagine smaller grains acting as restrictions for the compressive load applied on it, but the number of small grains may not be sufficient in number to have any observable difference in the tensile strength.

This difference is perhaps indicated by the slight advantage in the macrohardness of the Mg300 compared to Mg250. On the other hand, the slightly lower microhardness could also be an indication of the wider spectrum of grainsizes of the Mg300 compared with Mg250, with Mg300 having larger maximum grain sizes compared to Mg250.

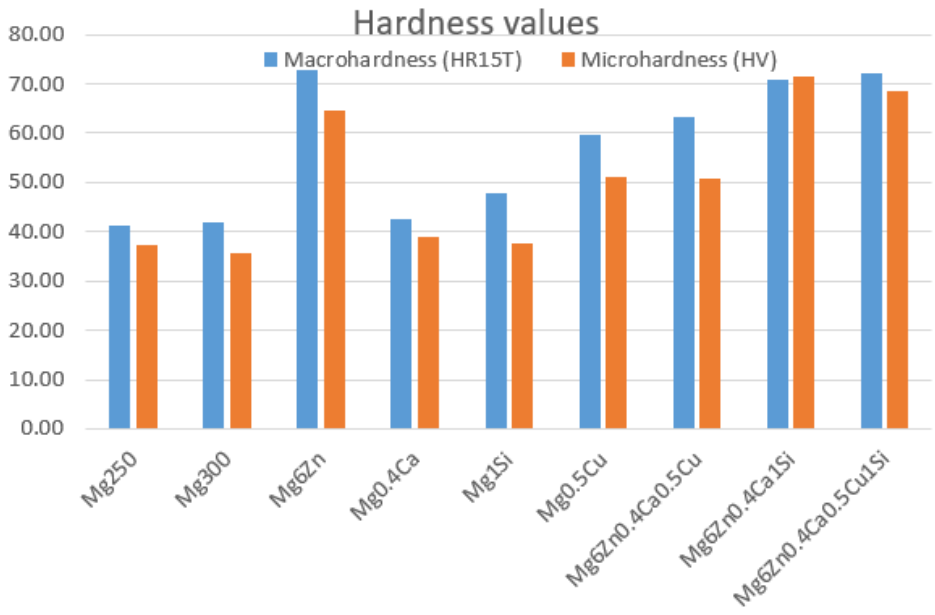

Figure 11: Macro hardness and Microhardness test results.

During the extrusion process, the particles are expected to undergo heavy loading leading to plastic deformation. During this deformation, the yielding need not occur at every particle at the same time. The orientation of the crystal structure of the Mg grains within the particles would determine the direction of slip and therefore the direction and degree of deformation of the particle. As seen from the optical micrograph, some of the particles are deformed more than others and those that are severely deformed seem to act as a mesh of sorts, helping to bind the other particles together while accommodating the necessary

deformation themselves. The general characteristics of the Mg particle deformation is relevant for all the other developed alloys as well.

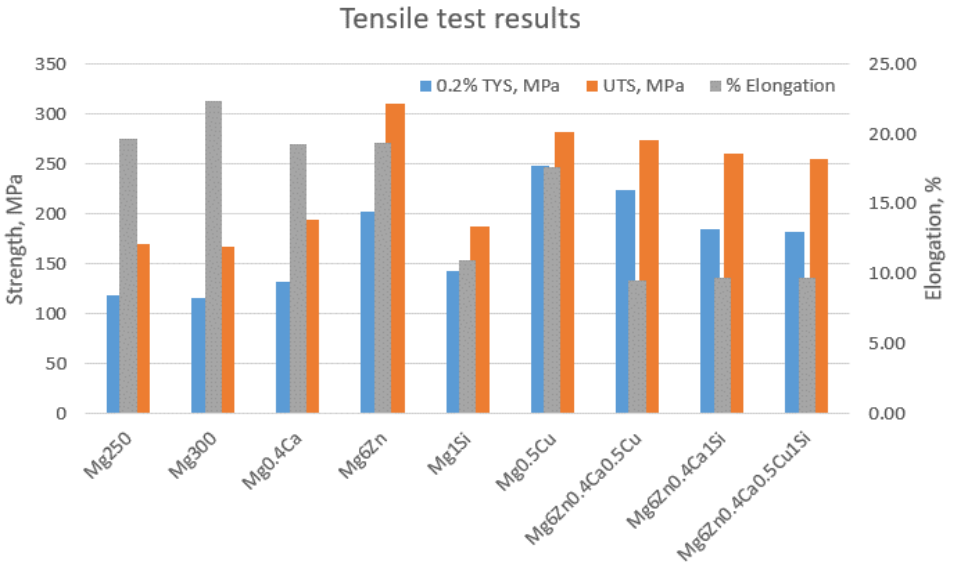

Figure 13: Room temperature Tensile test results.

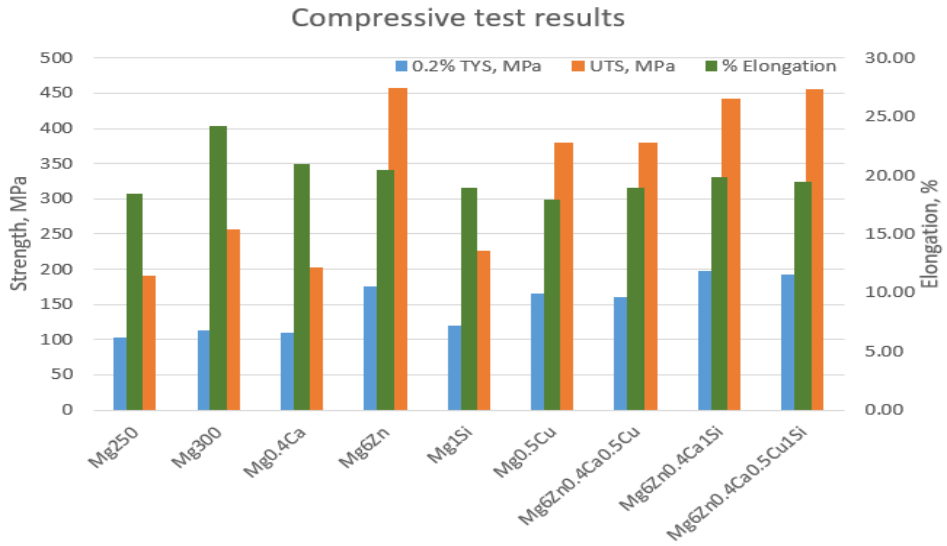

Figure 12: Room temperature compressive test results.

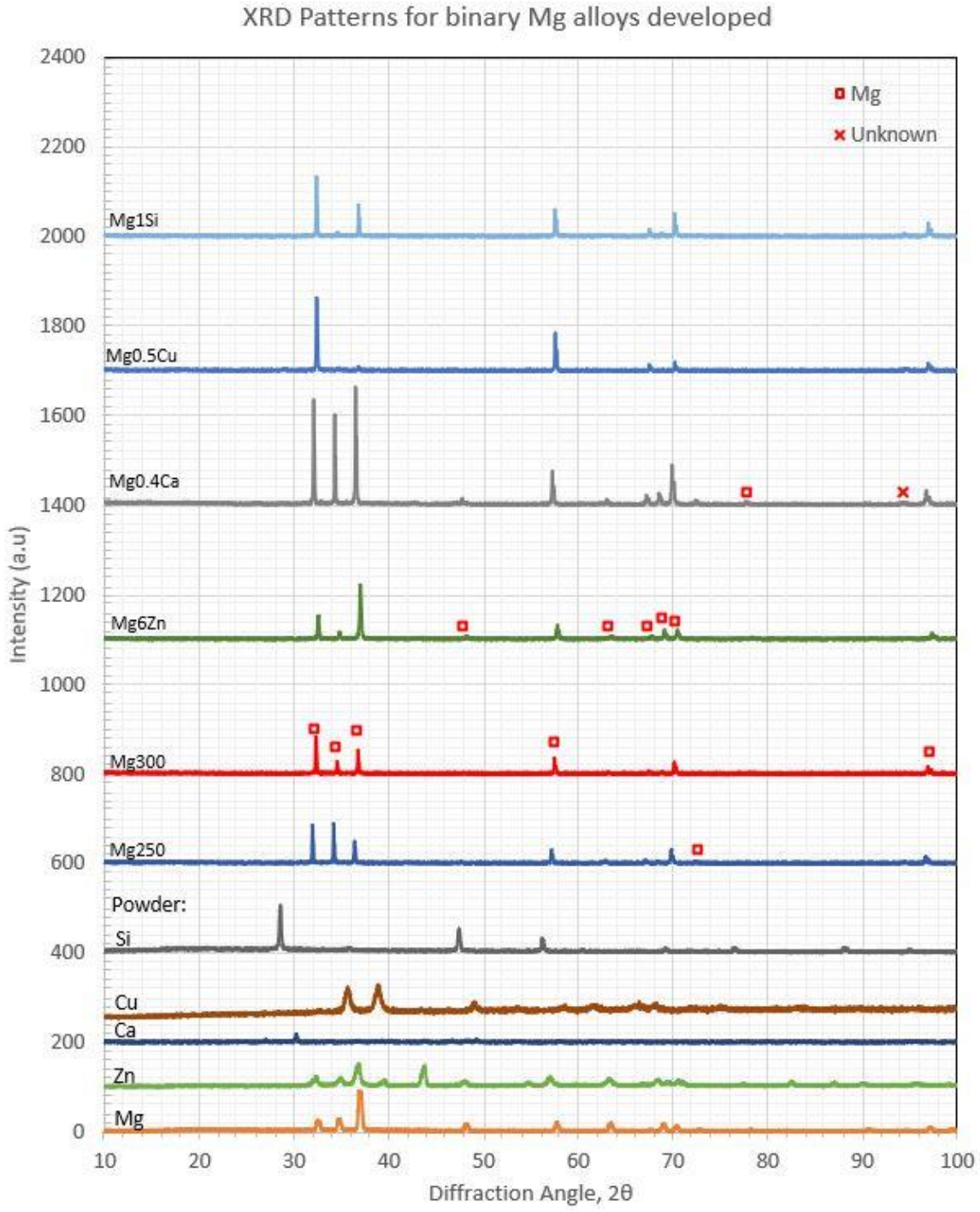

Figure 14: XRD Patterns of the binary alloys compared with the unalloyed Mg (sintered at 250°C and 300°C) and the element powders.

4.2.2 Effect of Zn:

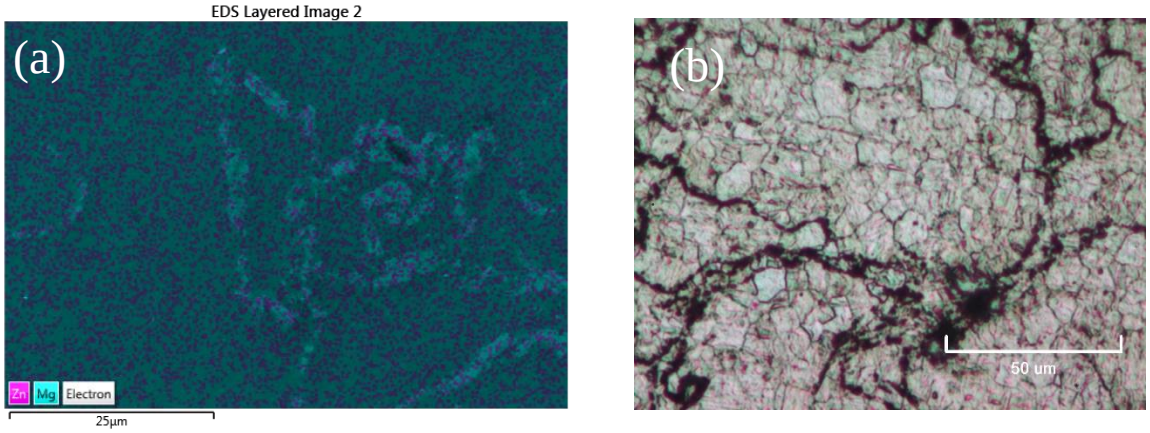

Figure 15: Image (a) shows the layered image of the EDX area map of Mg6Zn alloy and (b) shows the etched micrograph of the Mg6Zn alloy showing grains.

The distribution of Zn in the Mg matrix is well and uniform, although it is possible that it forms intermetallics and is present in the particle boundary as well, however, presence of any secondary phase produced in binary Mg alloy was not positively identified in XRD analysis. The sintering temperature being held at 400°C before raising it to 500°C allowed the Zn to diffuse into the Mg as well as form intermetallic with Mg.

The microstructural characterization of Mg-6Zn alloy shows that there is good interfacial bonding between the particles as seen in the EDX area map (Figure 15a). Uniform distribution of Zn is achieved in the binary alloy while in the presence of other elements, the distribution of the Zn in Mg is fairly uniform also (Figure 15a) with isolated regions of high Zn in the particle boundaries. Aside from that, there are regions of high Zn within the particles which could mean that there is an accumulation of Zn in the grain boundaries as well.

Etched optical micrograph shows the presence of near equiaxed grains with a spectrum of grain sizes (Figure 15, Figure 10). The average grain size of the binary alloy was found to

be about 4.2μm. In comparison, similarly produced unalloyed Mg had grains of average size 9.58μm, showing the grain refinement capability of Zn.

Of all the alloys produced, the 6 wt.% Zn provided the most increase in strength of all the elements. Especially exceeding in CYS (54.2%) and UCS (78.7%) (Figure 12). The uniform dispersal and the solid solution formed in the binary Mg6Zn via the diffusion of Zn solute into the Mg solid solution is likely the reasons for this. This diffusion would have created the presence of solute atoms inside the Mg. And the diffusion of Zn into the Mg particle albeit being present in the grain boundaries could be a result of trace amounts of intermetallic secondary phases formed. The presence of these trace amounts of secondary phase would inhibit the growth of any crystals during DRX, effectively allowing for grain boundary pinning mechanism leading to grain refinement [104].

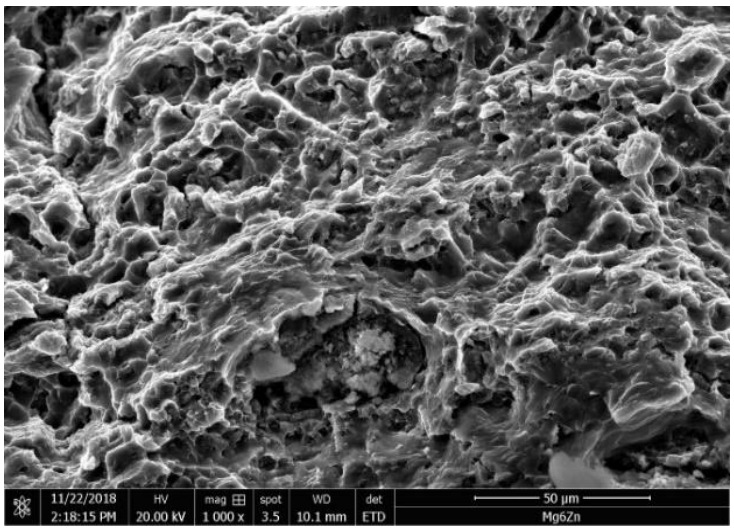

Figure 16: Tensile fractography of Mg6Zn alloy.

Aside from the solid solution strengthening and the possible precipitation strengthening, the grain refinement is effective in strengthening as well as improving ductility. This strengthening mechanism is also known as Hall-Petch strengthening. The significant grain refinement is also likely the reason for there being no significant drop in ductility despite

the significant improvement of strength as demonstrated by the Mg6Zn. Additionally, the presence of larger amounts of grain boundaries in addition to solid solution strengthening would likely be the prime causes of improved hardness resulting from the addition of Zn (Figure 11).

Fractography of the Mg6Zn alloy shows (Figure 16) a mix of brittle and ductile fracture with visible dimples.

4.2.3 Effect of Ca:

Ca diffusion into the Mg particle is observed with a fairly uniform distribution and discrete clusters around the particle boundaries and inside the particles (Figure 17). These clusters could be either unalloyed Ca or possibly a secondary phase such as Mg_2Ca. However, inside the particles, regions of sparse to no Ca, enclosed by Ca rich regions (Figure 17a) suggest the presence of Ca in grain boundaries. This is not surprising since Ca has a limited solubility in Mg with maximum solubility reaching 1.38 wt.% of Ca [105]. However, the presence of any secondary phase produced in binary Mg alloy was not positively identified in XRD analysis, although peaks matching possible secondary phase does overlap with some of the peaks of Mg. The low content volume of the Ca could also be a reason for any secondary phases produced to be below the limit of detection in XRD.

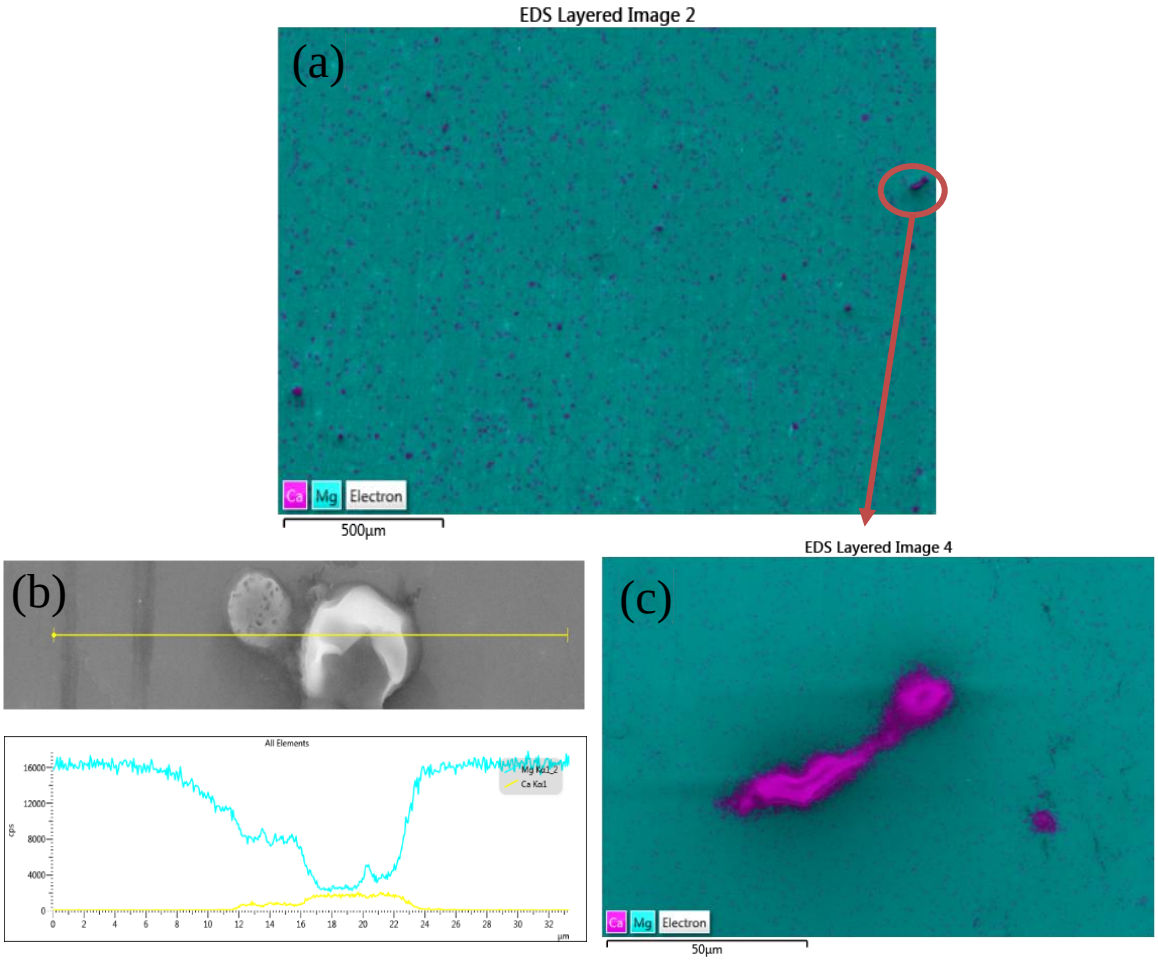

Figure 17: Image (a) shows the distribution of the Ca in Mg while (c) shows a magnified image of (a) showing the presence of the Ca particle in the Mg0.4Ca alloy and (b) shows the EDX line scan across a Ca rich particle which could be an intermetallic particle.

The etched optical micrograph of the Mg0.4Ca (Figure 18) does not indicate grain refinement of Mg other than a slight decrease in the maximum grain size of unalloyed Mg. This goes against the reported grain refinement properties of Ca in literature [70]. As mentioned earlier, the presence of discernible Ca rich continuous regions surrounding Ca scarce regions suggest their preferred presence in the grain boundaries after extrusion.

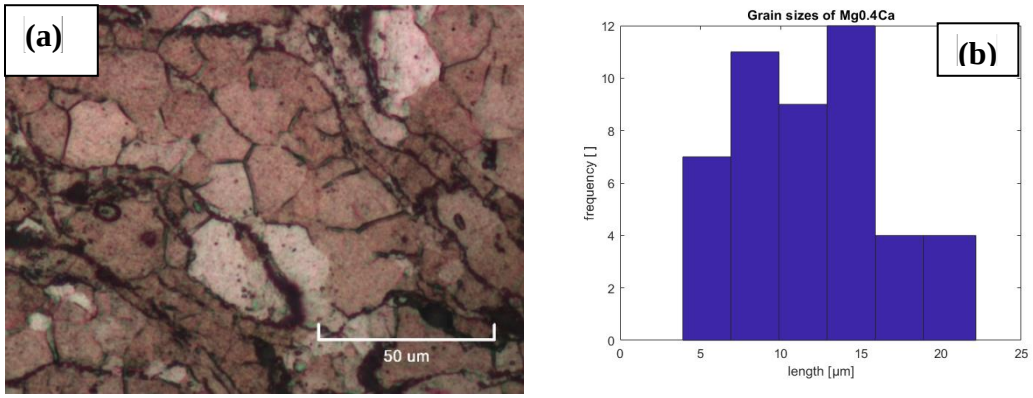

Figure 18: (a) Etched optical micrograph of Mg0.4Ca. (b) Histogram showing the grain sizes of Mg0.4Ca alloy.

Since neither the Ca nor the Mg particles melt, only solid solution diffusion is expected to occur during sintering. Therefore, it is possible that whatever Ca infiltrated into the particles occurred mostly during the hot extrusion process when the Mg was undergoing DRX and the Ca preference to the high energy grain boundaries. This would indicate that there were not much Ca to inhibit the forming grains except after the grain nucleation has progressed somewhat. This would explain the reduction in the maximum grain sizes of Mg by Ca.

As can be seen with the hardness values of Mg0.4Ca (Figure 11), there is only a slight increase in macrohardness and a noticeable increase in the microhardness. These results can be a result of Ca being softer than Mg and the macrohardness indentation encompassing a larger area would be overlapping with the particle boundaries and grain boundaries and would normally be higher in the presence of higher hardness components in these regions. However, with Ca being softer than Mg, any clusters of Ca in these regions would not be additive to the hardness, and the slight increase could be due to presence of small amounts of secondary phases present. The presence of harder secondary phases with

a preference in grain boundaries would be in agreement with the increase in micro hardness as well as the EDX area mapping as discussed above.

In terms of strength under tension, adding 0.4 wt.% Ca lent an increase in a 13.9% of TYS and a 16.8% increase in UTS after a loss of about 14% in ductility (Figure 13). However, the strength of the Mg0.4Ca alloy in compression was detrimental compared to unalloyed Mg in all parameters of concern, and especially the drop in about 21% UCS is significant (Figure 12). These results suggest possible embrittlement of the alloy attributed to the Mg_2Ca phase [54]. The slight increases of strength in tension could be indicative of small amounts of diffusion of Ca leading to solid solution strengthening effects.

Fractography of the binary alloy Mg0.4Ca shows the visible crack propagated through the particle boundaries and visible cleavage facets (Figure 19).

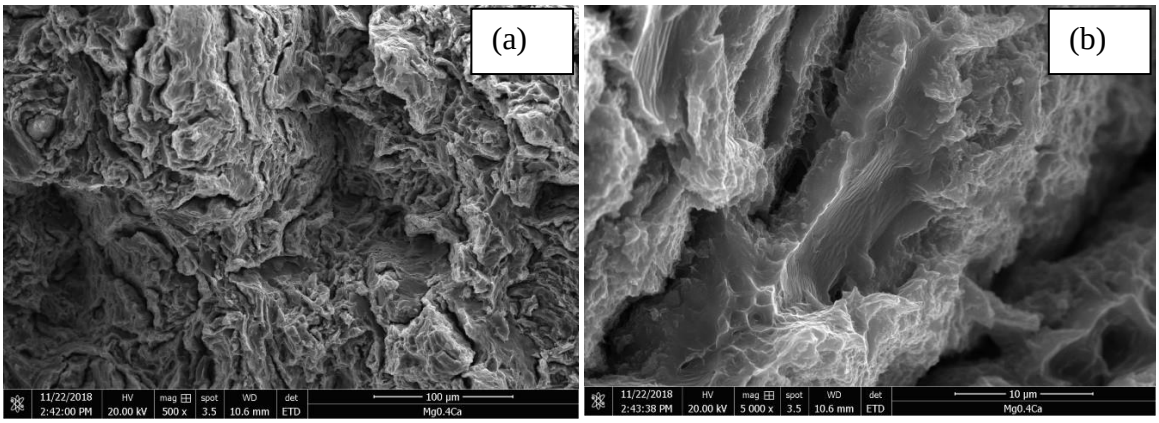

Figure 19: Tensile fractography of Mg0.4Ca showing brittle fracture and pseudo-dimples and trans granular cracking.

4.2.4 Effect of Si:

The presence of Si in the Mg1Si alloy is mostly confined to the particle boundaries with some diffusion of Si into the Mg particle (Figure 20). Optical micrography of etched Mg1Si shows blue colored Si rich regions within the particle boundaries present in discontinuous aggregates. This observation is supported by the EDX area mapping (Figure 20a) done on the alloy. However, the EDX area mapping also showed Si diffusion into the particle and their presence in seemingly continuous boundary regions enclosing areas of Si scarcity. This could imply the presence of Si in the grain boundaries.

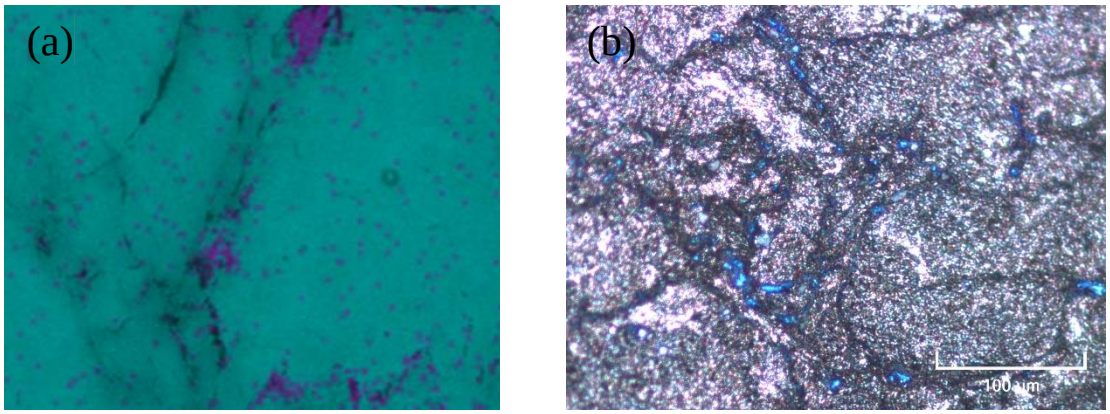

Figure 20: Image (a) shows a magnified image of the EDX area map of the Mg1Si alloy and (b) shows the optical metallography image of Mg1Si with Si (blue) visible in between particles.

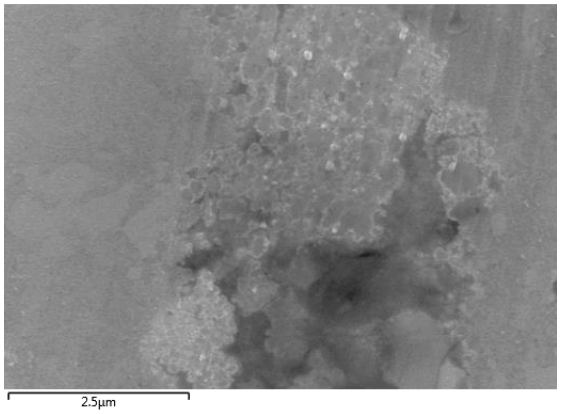

Figure 21: Shows the interface region between the Mg particles.

The average grain sizes of the Mg1Si compared with unalloyed Mg was reduced, demonstrating the grain refinement ability of the Si in Mg. This grain refinement is possibly due to the presence of diffused Si inhibiting the advance of the grain growth during DRX thereby effectively pinning the grain boundary.

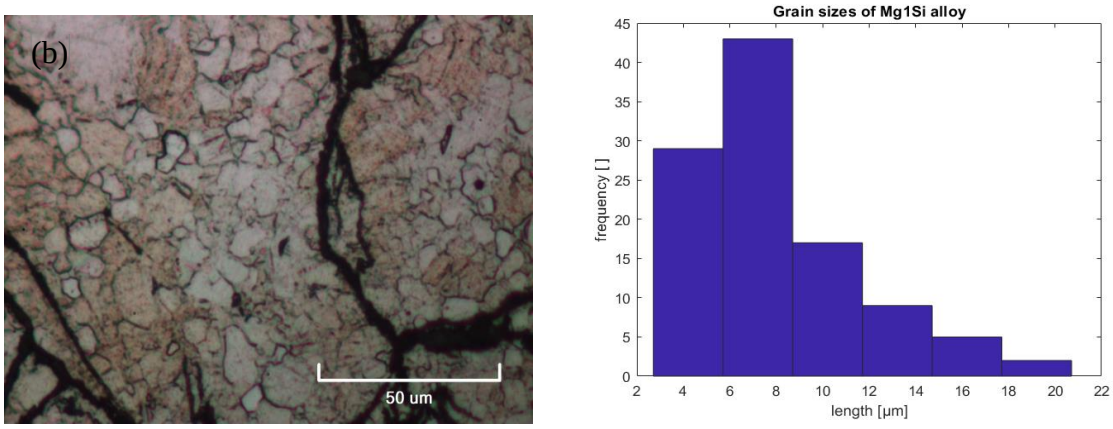

Figure 22: Histogram of grain sizes in the Mg1Si alloy.

These observations are in agreement with the hardness results obtained for Mg1Si alloy. The macrohardness is observably improved (14.6%) compared to unalloyed Mg whereas the microhardness was only improved by about 5.2%. Again, this difference is probably due to the macrohardness indentation by the 1/16th inch hardened steel ball encompassing a wider area encompassing hard particle boundaries made harder than unalloyed Mg by the presence of hard Si.

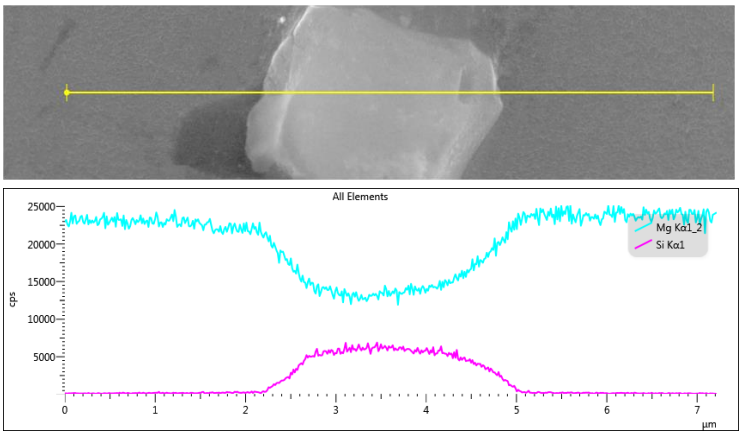

Figure 23: EDX line scan across a particle with both Mg and Si present.

Despite a modest increase in TYS and UTS, the reduction in ductility of Mg by half shows that addition of 1 wt.% Si embrittles the Mg. This embrittlement of the alloy is seen to reduce the compressive strength of the alloy. Various literature talks about the formation of hard secondary phase of Mg_2Si being the cause of it. Though the presence of this phase was not observed positively by XRD (Figure 14), particles indicative of such a composition was observed via the EDX line analysis (Figure 23). However, even without the presence of secondary phases, Si is in itself harder than the Mg and its clusters observed in the particle boundaries and its likely presence in the grain boundaries would act as hard particles which could act as stress concentrators for cracks to initiate and propagate. Additionally, Si has a diamond lattice structure which would make it more resistant to accommodate deformation. Perhaps because the stress concentration effects around the hard particles is more prominent when a compressive load is applied that it resulted in a decrease in UCS of the Mg alloy as compared with unalloyed Mg. Another possibility is that the segregation of the Si with preference to form oxides in the particle boundaries could have resulted in insufficient interfacial bonding between the interparticle Si and the

rest of the Mg matrix. The weak interfacial bonding is observed in the SEM image (Figure 21).

4.2.5 Effect of Cu:

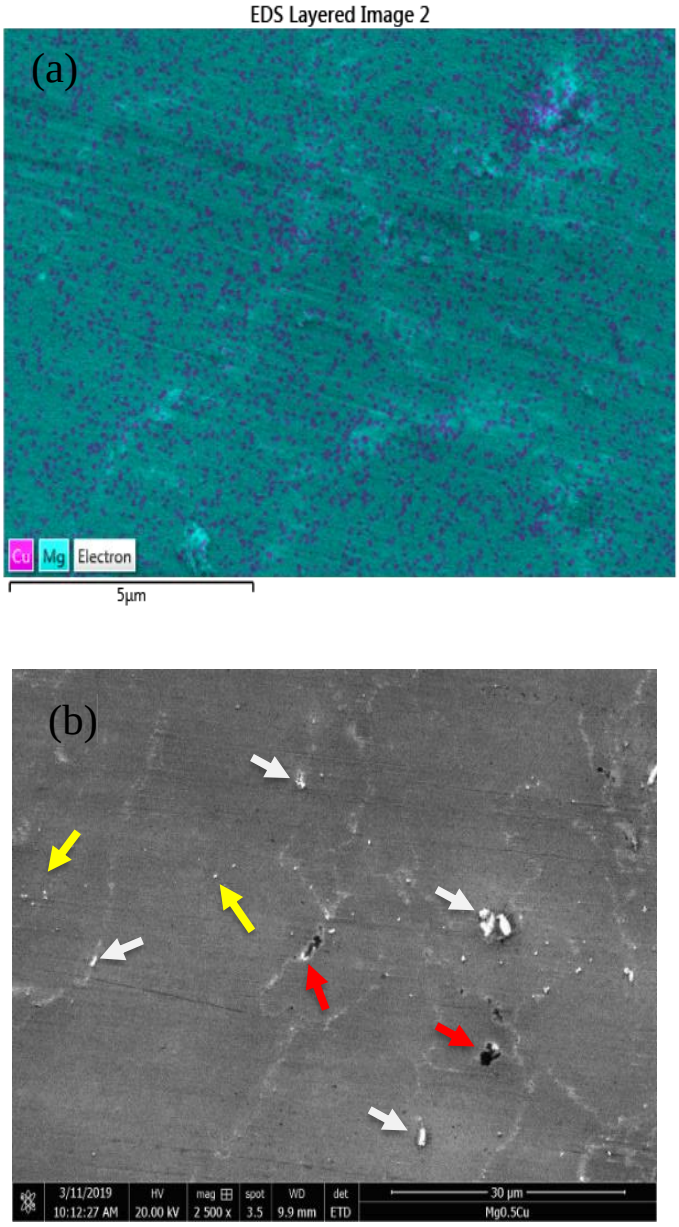

Figure 24: (a) Shows the EDX layered map showing good Cu distribution and (b) shows the SEM image of Mg0.5Cu showing the presence of Cu in clusters around the particle boundary (white arrows), inside the particles (yellow arrows) and the voids left behind of vacancy presumably of secondary phase (red arrows).

The microstructural characterization of Mg0.5Cu alloy shows that Cu is well dispersed in the Mg matrix with some clusters of Cu in isolation (Figure 24). At a sintering temperature of 500°C it is well below the melting temperature of either the Mg or Cu and so only solid-solid diffusion is expected to take place. The diffusion of Cu into the Mg particle, and the grain boundary is observed via the EDX Area mapping (Figure 24a). Though similar to Ca and Si, as discussed above, regions of Cu scarcity surrounded by regions enriched with Cu exist, it does so to a lesser extent than those elements and the diffusion of Cu into the Mg matrix creating a solid solution is suggested by this. This formation of solid solution is further identified by the shifts in the Mg peaks of the XRD (Figure 14) for Mg0.5Cu.

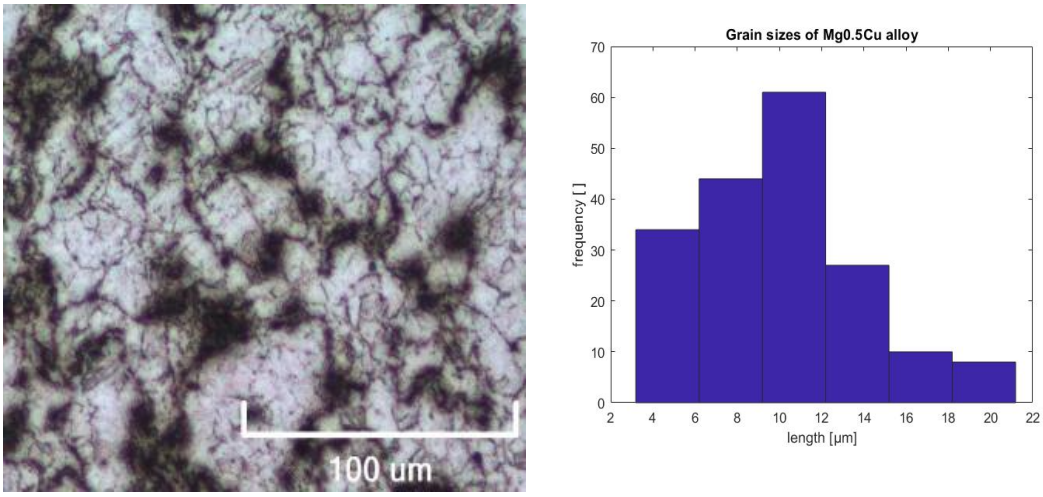

Figure 25: Micrograph of etched Mg0.5Cu alloy. (b) Histogram of the grain sizes in Mg0.5Cu alloy (obtained using Linecut Matlab program).

The grain sizes of the binary alloy Mg0.5Cu do not suggest particularly strong ability of the Cu in grain refinement of the Mg (Figure 10, Figure 25) except that it limits the maximum size of the grain size of the Mg matrix. These results possibly indicate as similarly discussed for Ca and Si, that the bulk of the diffusion takes place during the plastic deformation phase and that the diffusion during sintering is only at the particle borders. It has been reported by J. Dai et al. [106] that the diffusion co-efficient of Cu impurity in Mg

is lower than the Mg diffusion into Cu, thereby favoring the diffusion of Mg into Cu. This would explain the lack of significant grain refinement except to limit the maximum size, whereby the diffusion of Cu does take place into the forming grain boundaries after nucleation has progressed and DRX is already taking place. Grain boundaries are reported to be high diffusivity paths owing to higher mobility of the solute atoms along the grain boundary defects compared to the lattice [107].

Both the macrohardness and microhardness is higher than the unalloyed Mg, representing further evidence of Cu diffusion into the Mg particle and possible solid solution strengthening. The macrohardness, owing to its wider indentation is higher than the microhardness as discussed with previous elements.

The TYS of Mg on addition of 0.5 wt.% Cu increased by about 113% and the UTS improved by about 69% while still having considerable ductility (17.67%) (Figure 13). Similarly, both the CYS and UCS was also increased (45.4% and 48.5% respectively) with a decrease in ductility of about 25.6% (Figure 12) to achieve similar ductility as in tension i.e. 17.97%. These results indicate a strengthening mechanism which as discussed above, is perhaps due to solid solution strengthening. The good interfacial bonding between the particle boundary and the particle as seen in Figure 24 is also a reason to inhibit particle debonding under load. Unlike Si, Cu has a hardness value which is only slightly higher than Mg and has an FCC lattice structure which allows it to accommodate deformations much easier than the diamond structure of Si.

4.3 Discussion on the developed Mg Alloys

The two quaternary alloys and the ternary alloy developed has strengths far exceeding that of unalloyed Mg. Since the elements used have been vetted for their individual biocompatibility and degradation inside the human body, the alloys developed are expected to be fully bio-degradable Mg alloys.

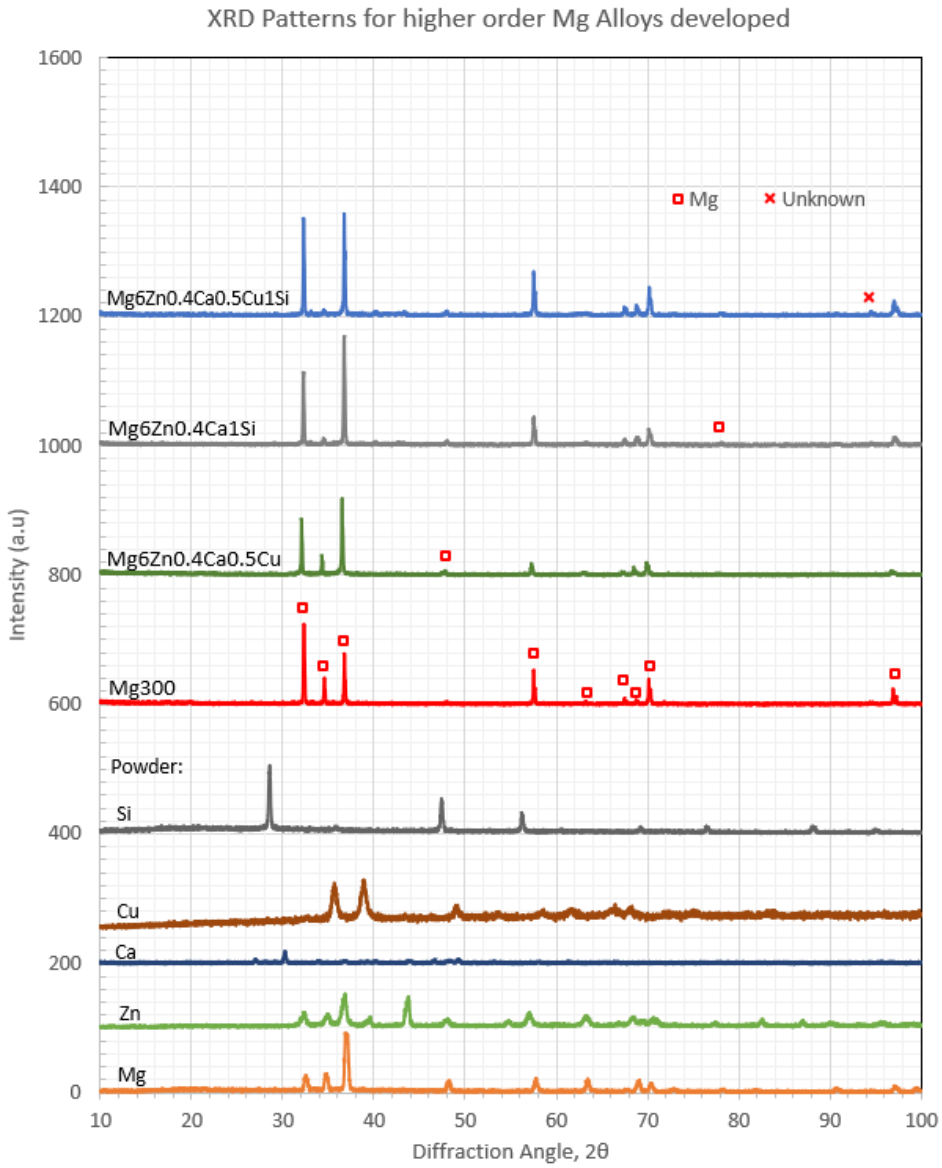

Figure 26: XRD Patterns of the developed ZX alloys compared with the starting powders and the unalloyed Mg.

Especially the alloy Mg6Zn0.4Ca0.5Cu is a very promising Mg alloy with strength far exceeding that of reported Mg alloys [108].

Mg6Zn0.4Ca0.5Cu alloy with the highest UTS for the higher order alloys is a suitable high strength alloy of Mg [108]. The other higher order alloys are also highly competitively strong. However, the highest UTS and UCS with a significantly high ductility is found to be Mg6Zn. Future work in the field of biodegradable Mg alloys could benefit in concentrating on this simple alloy produced via Blend-Press-Sinter method.

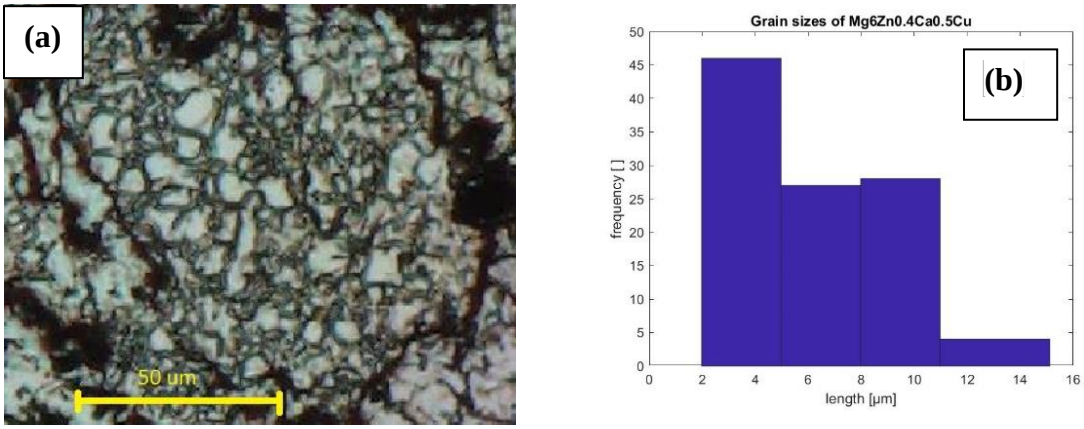

Figure 27: (a) Etched optical micrograph of Mg6Zn0.4Ca0.5Cu and (b) Histogram showing the grain sizes.

The microstructural characterization of the Mg6Zn0.4Ca0.5Cu alloy shows that there is an accumulation of alloying elements in the particle boundaries, with diffusion of these elements into the Mg particle during sintering. This solid-state diffusion has led to the large grain refinement in the Mg and formed a solid solution. The peak shifts in the XRD pattern support this conclusion.

The microalloying in Mg6Zn0.4Ca0.5Cu resulted in significant grain refinement of the Mg particle which is due to the gradient solid solution produced. The significantly high macro

and micro hardness results could be due to the concentrated solid solution and grain refinement induced by it.

Interparticle crack propagation in the unalloyed Mg could be due to the pile up of moving dislocation at the Mg particle boundaries. In the Mg6Zn0.4Ca0.5Cu alloy, the presence of accumulations of the elements at the interparticle boundary with strong bonding to both the Mg particles and to each other could act to provide dislocation relief. This is also supported by the larger work of fracture i.e. the energy absorbed by the alloy before fracture and as seen with the tensile fractographic image (Figure 29a).

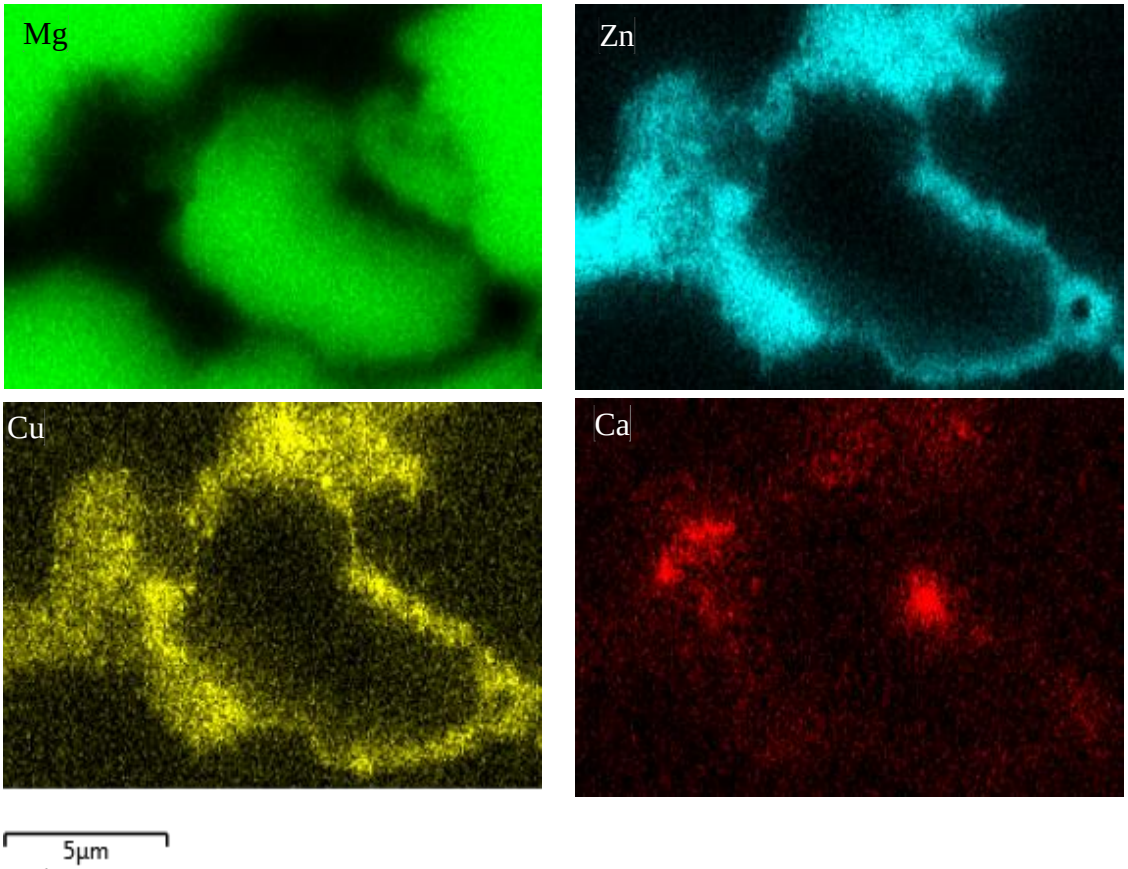

Figure 28: EDX mapping of the surface of Mg6Zn0.4Ca0.5Cu alloy showing the distribution of the elements.

Yield strength of magnesium is the stress that the material can undergo before dislocation slip and tensile twinning starts. The grain refinement leading to presence of a large number of grain boundaries and the solid solution formed due to the alloying elements are expected to resist the dislocation slip and deformation twinning which is a reason for the strain hardening effect resulting in the higher UTS after yielding.

The XRD analysis of the Mg6Zn0.4Ca0.5Cu (Figure 26) showed that there was no positively identified presence of either the intermetallic secondary phases or individual

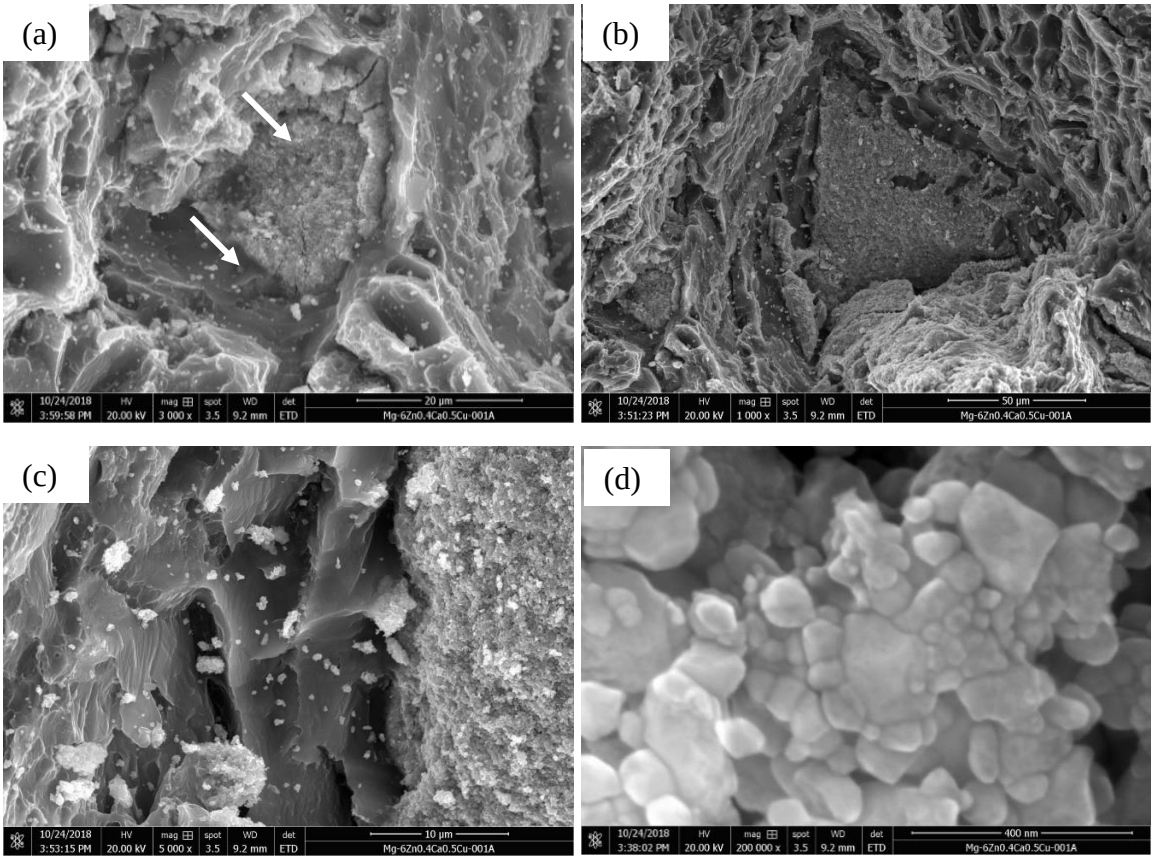

Figure 29: Tensile fractography of Mg6Zn0.4Ca0.5Cu with (a) showing the accumulated alloying elements with the arrows showing crack propagation through it while (b) shows the ductile dimples in the Mg solid solution. (c) shows the interface bonding between the Mg particle and the accumulated alloying elements and (d) shows the fracture of accumulated alloying elements.

alloying elements. This could be due to the small volume of both in comparison to the bulk α-Mg.

The microstructural characterization of the Mg6Zn0.4Ca1Si alloy shows that the ZX alloy with the addition of Si preserves the diffusion ability of Zn as compared to Mg6Zn (as discussed above). The Si, unlike the Cu (as discussed above) does not seem to inhibit the diffusion of Zn is illustrated in the uniform diffusion and distribution of the Zn in Mg similar to that of the binary Zn effect on Mg. This is perhaps because, unlike Cu, Si does not form intermetallic phases with Zn and as such, all the Zn is available to diffuse into the

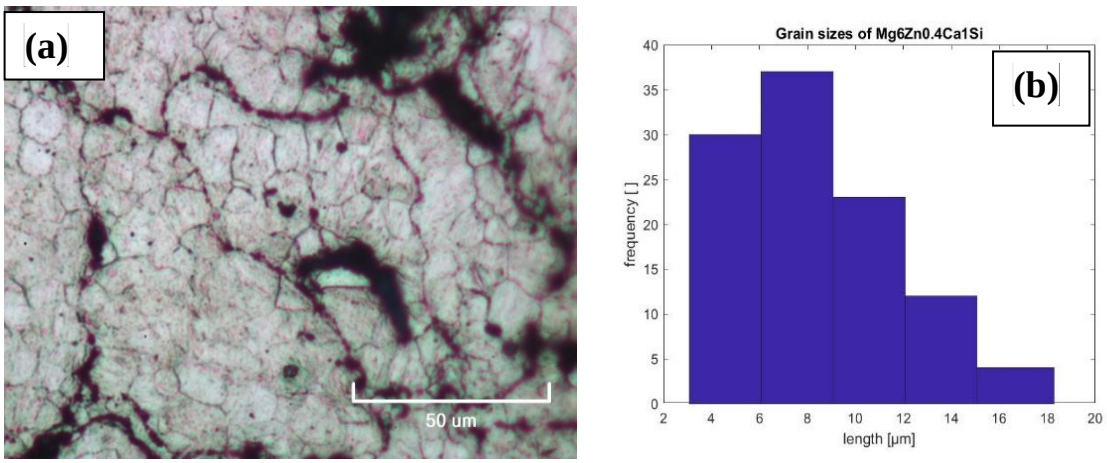

Figure 30: (a) Etched optical micrograph of Mg6Zn0.4Ca1Si and (b) Histogram showing the grain sizes.

Mg unrestricted. The diffusion of Si into the Mg is also observed, with clusters of it present around the Mg particle boundaries. Cluster formation around the particle boundary has also been observed for Ca. The presence of seemingly empty areas surrounded by a ring of element rich region inside the Mg particles suggest that Si and Ca was more in the grain boundaries than in the bulk α-Mg of the grains.

The macro hardness of the Mg6Zn0.4Ca1Si shows that it has a high hardness of about 70 (HR15T) and has microhardness higher than all the other alloys (71.61 HV). This could be

due to the uniform distribution of the hard particles and/or hard secondary phases. The results of hardness higher than that of binary alloys indicate the presence of hard intermetallic secondary phases and their uniform distribution could be the result of high microhardness as well. However, the presence of secondary phases was not detected by XRD analysis (Figure 26), perhaps due to the small volume fractions of those individual phases even if present.

The Ultimate tensile strength (UTS) of the Mg6Zn0.4Ca1Si alloy was about 56% higher than that of unalloyed Mg (Figure 13) while compromising on ductility, which was about 56.6% lower. On the other hand, Mg6Zn0.4Ca0.5Cu1Si had UTS about 52.7% higher than that of unalloyed Mg with a loss in ductility of about 56.5%.

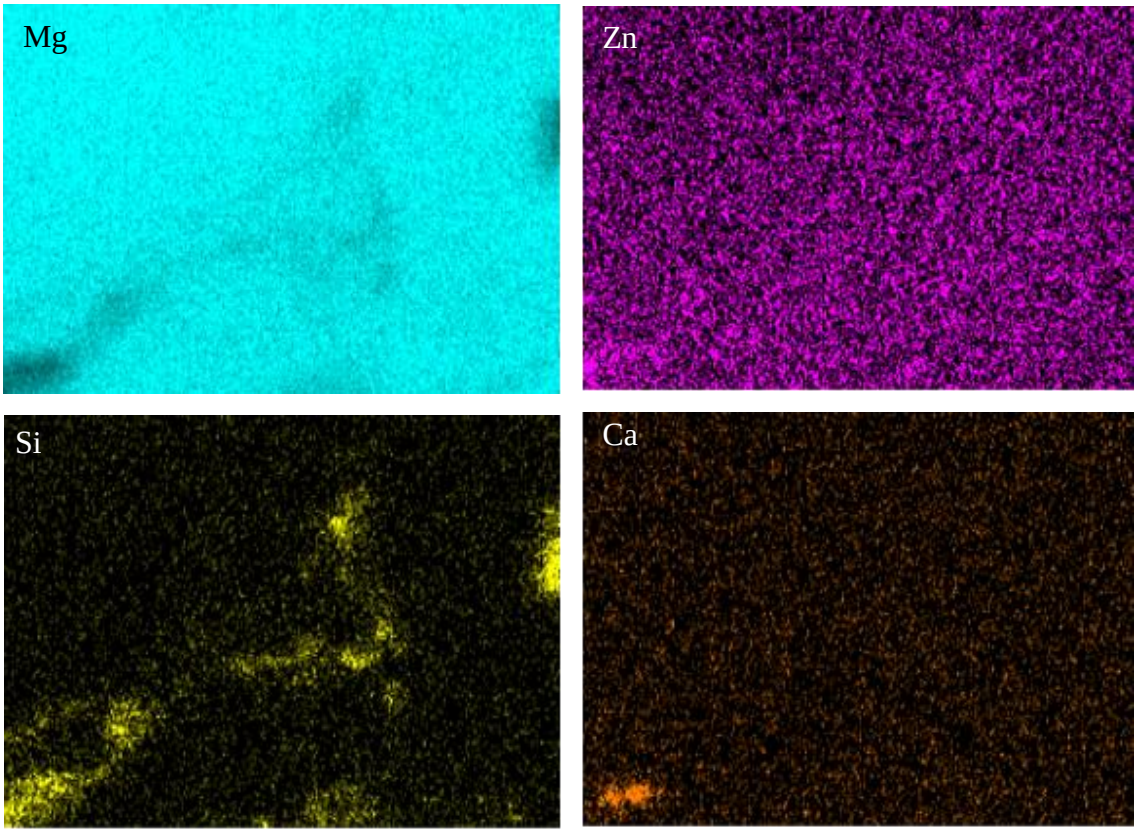

Figure 31: EDX mapping of the surface of Mg6Zn0.4Ca1Si alloy showing the distribution of the elements.

However, the compressive yield strength (CYS) of these two alloys were found to be the highest among all the alloys produced (Figure 12). This could be due to the presence of clusters of hard phase particles and/or hard alloying element clusters which could act as reinforcement similar to that in a composite. It has been reported [109] that in Mg composites, the addition of reinforcement restricts the twin nucleation and propagation resulting in delayed yielding. This would also explain the significantly reduced ductility due to restricted twinning.

Unlike the Mg6Zn0.4Ca1Si, the Mg6Zn0.4Ca0.5Cu1Si shows the clustering of the Zn at the particle boundaries despite the diffusion of Zn into the Mg. Si is mostly clustered around the particle boundaries as has been discussed above. Ca and Cu also both show similar clustering around the particle boundaries with some presence inside the Mg particles (presumably more so around the grain boundaries than with the other alloys discussed above). Comparison with the other ZX alloys above, it can be concluded that the presence of Cu restricts the diffusion of other elements into the Mg. This could be due to Cu readily forming intermetallic phases with the other elements, making the amount of elements available for diffusion less. A lesser concentration of the elements available for

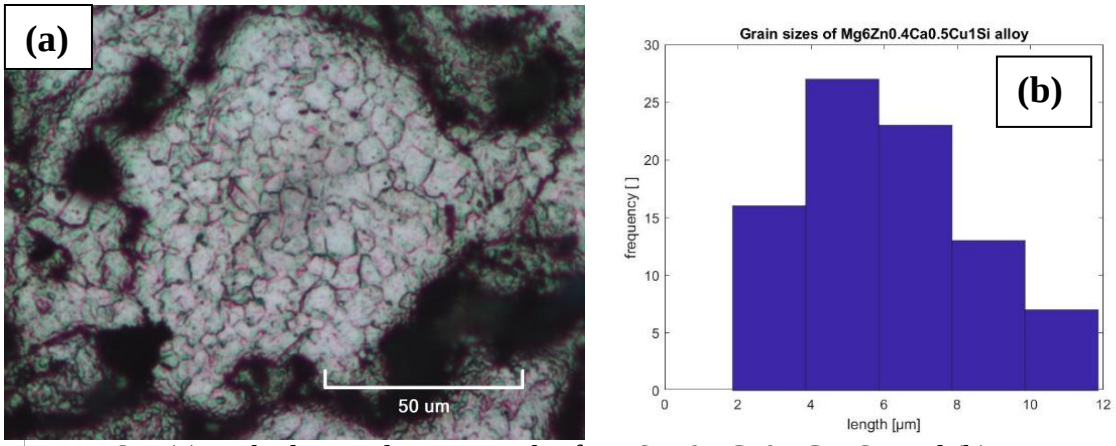

Figure 32: (a) Etched optical micrograph of Mg6Zn0.4Ca0.5Cu1Si and (b) Histogram showing the grain sizes.

diffusion would explain the clustering of the elements around the particle boundary and progressively less being available for diffusion into the Mg. The lower available concentration could also be the reason that there was no or limited diffusion into the grain.

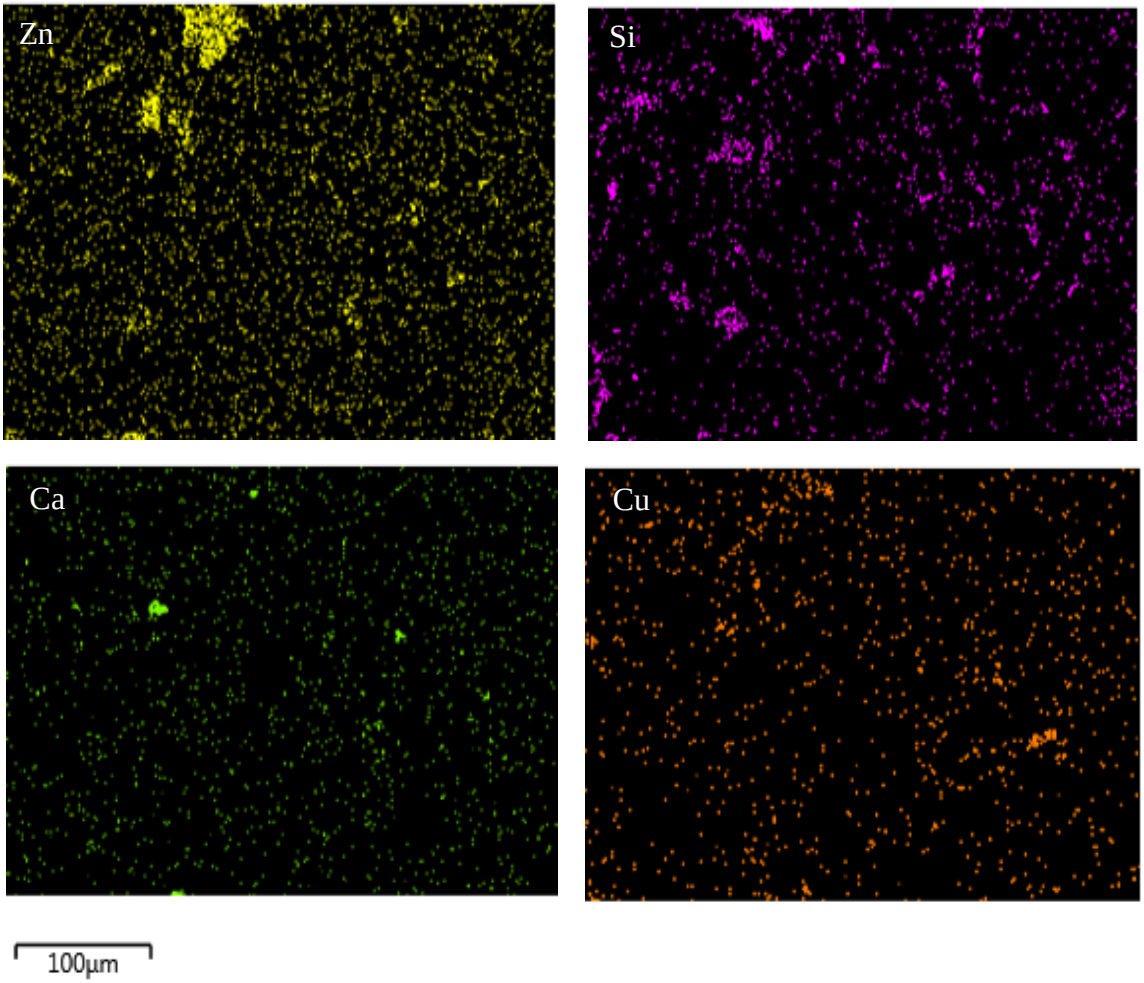

Figure 33: EDX mapping of the surface of Mg6Zn0.4Ca0.5Cu1Si alloy showing the distribution of the elements.

The microstructure of Mg6Zn0.4Ca0.5Cu1Si shows that Zn have diffused into the Mg matrix with some intermetallic secondary phases in the particle boundary.

The tensile fractography of the ZX alloys (Figure 34) show that there was crack propagation through the particles and the presence of intergranular cracks.

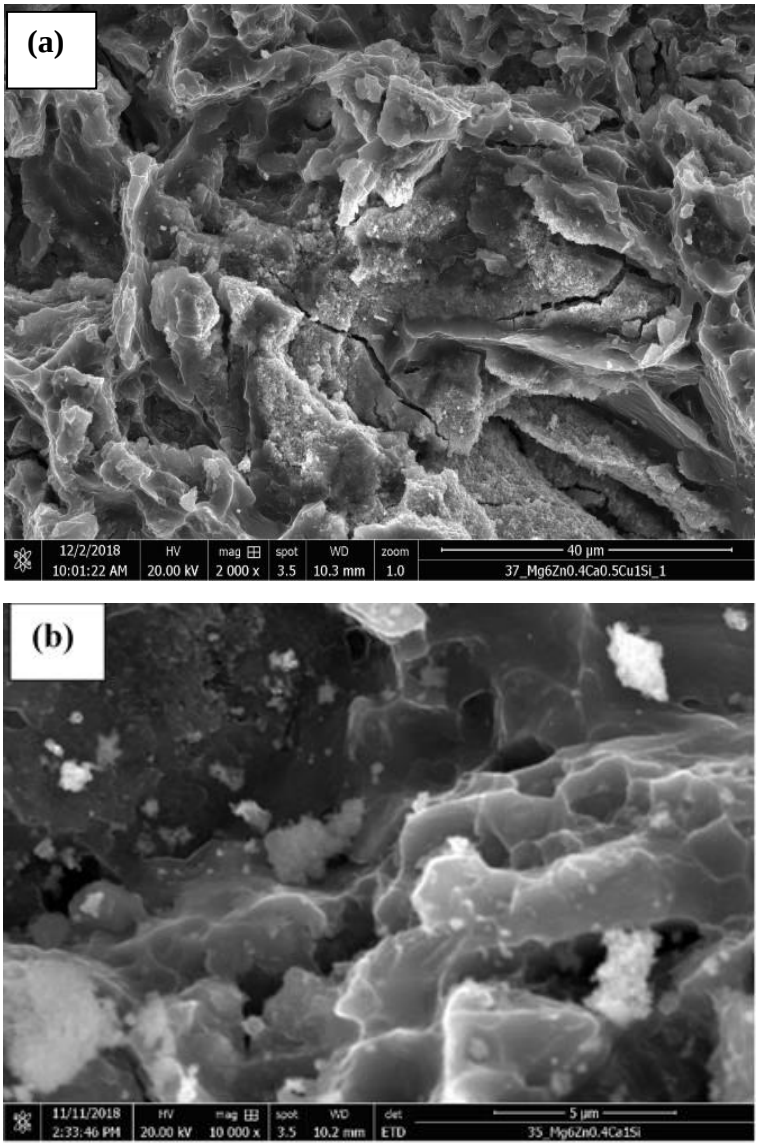

Figure 34: Representative Tensile fractography for both the alloys show (a) interparticle cracking and trans-particle cracking in Mg6Zn0.4Ca0.5Cu1Si and (b) the intergranular cracks as demostrated by Mg6Zn0.4Ca1Si alloy.

The compressive fractography of the ZX alloys show the presence of the clusters of the powders along the fracture surface. The clusters in this case could be the primary inhibition to the shear of the fracture surface contributing to the high compressive strength of these alloys.

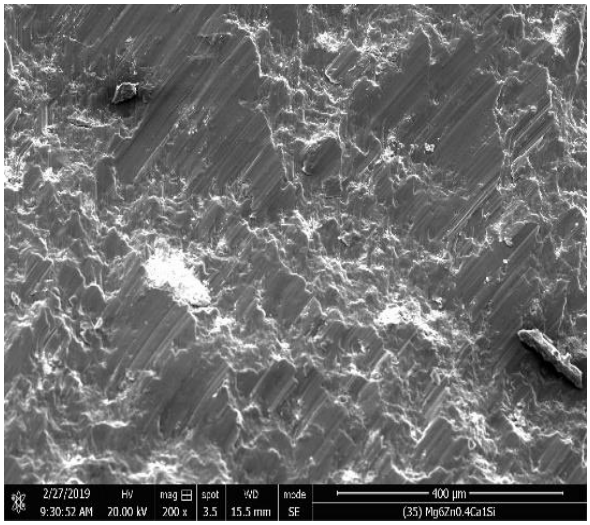

Figure 35: Compressive fracture surface of Mg6Zn0.4Ca1Si showing cluster powders on the fracture surface.

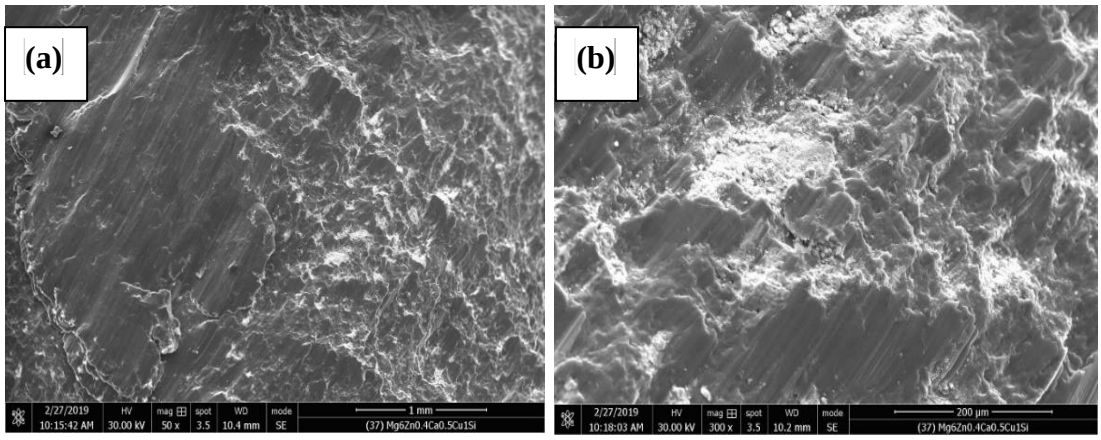

Figure 36: Compressive fractography of Mg6Zn0.4Ca10.5CuSi alloy shows clusters of powders on the fracture surface.

CHAPTER 5

CONCLUSION

Mg alloys with significantly high strength were developed using the Blend-Press-Sinter process followed by hot extrusion. It can be concluded that the process of Blend-Press-Sinter followed by Extrusion is suitable for the production of biodegradable Mg alloys with high strength and reasonably high ductility. The alloying elements chosen for this work (Zn, Ca, Cu and Si) were found in literature to be both biodegradable and biocompatible alloying elements of Mg. The effects of the four elements on the grain size and strength was investigated. The following conclusions can be made:

- The diffusion of the alloying elements is in general forming a gradient solid solution inside the Mg particle.
- The Zn diffuses and distributes into the Mg matrix on its own, however, in the presence of Cu the diffusion of Zn is affected, probably due to formation of intermetallic phases with Cu.
- Ca diffuses into the Mg matrix, with possible preference to the grain boundaries.
- Si has limited diffusion into the Mg particle and when it does, it could be in the grain boundaries. The bulk of it exists in clusters in the particle boundaries.
- Cu diffuses more readily into the Mg than either Si. However, its presence affects the diffusion of other elements due to possible intermetallic formation.
- The addition of Zn refines the grains of Mg and provides high strength to the Mg alloy.

- The grain refining ability of Ca, Si and Cu has not been seen in this study due to perhaps limited Solid-Solid diffusion.
- The Mg6Zn0.4Ca0.5Cu alloy has been found to be a very promising alloy which has good potential to serve as a biocompatible Mg alloy.
- The Mg6Zn0.4Ca1Si and Mg6Zn0.4Ca0.5Cu1Si both have very good yielding strength under compression.
- Mg6Zn and Mg0.5Cu alloys produced using the blend-press-sinter method are also very promising binary alloys with good tensile and compressive strength with sufficient ductility.

CHAPTER 6

RECOMMENDATIONS FOR FUTURE STUDIES

The scope of this Thesis was maintained within the stated objectives of studying the effect of Zn, Ca, Cu and Si on the Mg and the development of biodegradable Mg alloys. The biocompatibility of the elements was reviewed via existing literature. The development of high strength and sufficient ductility alloys have been developed in this Thesis, which needs additional research into the degradation characteristics of these alloys both in-vitro and in-vivo. Having said that, however, it should be noted that the high strength performance of the developed alloys should provide sufficient core strength for any biodegradable implant which could be enhanced for corrosion resistance via surface modification methods or the use of functional gradation. In such a case these present alloys would serve as high strength cores and would only be exposed to the corrosion media during the last stages of the healing.

The effect of extrusion on the BPS process route developed alloys have been studied here, however, future work could include ECAP process on the BPS produced alloys. With respect to the various literature, it is expected to produce a refined microstructure.

The experimental parameters used in this study were derived from similarly successful experimental processes with work mainly focused on Mg based composites. The work on Mg alloys may have different optimum parameters, which could be studied by those intending to study the influence of the parameters on the alloys produced. This includes

studies on the compaction pressure, sintering and extrusion temperature, extrusion ratio, etc.

The age hardening behavior and the effect of temperature post extrusion can be studied as an extension to this current study.

The Blend-Press-Sinter method for producing Mg alloys of various compositions and properties is promising due to the uniformity in distribution of the individual alloying element powders. Further studies could explore the effect of Mg-Zn-Cu based on this study, as Zn allows liquid-solid diffusion and Cu diffuses via solid-solid mechanism into the Mg. Of course, it could lead to an inhibition of Zn diffusion as seen in this study, however, the results would be interesting nonetheless.

Presently highest performance alloy compositions made by casting could be investigated for a good comparison of the effect of the processing route and could potentially provide better performance with the advantage of the better uniformity using BPS.

References

[1] F. Witte, “Reprint of: The history of biodegradable magnesium implants: A review,” *Acta Biomater.*, vol. 23, no. S, pp. S28–S40, 2015.

[2] Z. Sheikh, S. Najeeb, Z. Khurshid, V. Verma, H. Rashid, and M. Glogauer, “Biodegradable materials for bone repair and tissue engineering applications,” *Materials (Basel).*, vol. 8, no. 9, pp. 5744–5794, 2015.

[3] C. Rössig, N. Angrisani, P. Helmecke, S. Besdo, J. M. Seitz, B. Welke, N. Fedchenko, H. Kock, and J. Reifenrath, “In vivo evaluation of a magnesium-based degradable intramedullary nailing system in a sheep model,” *Acta Biomater.*, vol. 25, pp. 369–383, 2015.

[4] P. Han, P. Cheng, S. Zhang, C. Zhao, J. Ni, Y. Zhang, W. Zhong, P. Hou, X. Zhang, Y. Zheng, and Y. Chai, “In vitro and in vivo studies on the degradation of high-purity Mg (99.99wt.%) screw with femoral intracondylar fractured rabbit model,” *Biomaterials*, vol. 64, pp. 57–69, 2015.

[5] T. Yoshida, T. Fukumoto, T. Urade, M. Kido, H. Toyama, S. Asari, T. Ajiki, N. Ikeo, T. Mukai, and Y. Ku, “Development of a new biodegradable operative clip made of a magnesium alloy: Evaluation of its safety and tolerability for canine cholecystectomy,” *Surg. (United States)*, vol. 161, no. 6, pp. 1553–1560, 2017.

[6] M. Asgari, R. Hang, C. Wang, Z. Yu, Z. Li, and Y. Xiao, *Biodegradable metallicwires in dental and orthopedic applications: A review*, vol. 8, no. 4. 2018.

[7] S. H. Ye, Y. Chen, Z. Mao, X. Gu, V. Shankarraman, Y. Hong, V. Shanov, and W. R. Wagner, “Biodegradable Zwitterionic Polymer Coatings for Magnesium Alloy Stents,” *Langmuir*, 2018.

[8] W. D. Callister and D. G. Rethwisch, *Materials Science and Engineering: An Introduction*, 10th ed. John Wiley and Sons, 2018.

[9] D. Zhao, F. Witte, F. Lu, J. Wang, J. Li, and L. Qin, “Current status on clinical applications of magnesium-based orthopaedic implants: A review from clinical translational perspective,” *Biomaterials*, vol. 112, pp. 287–302, 2017.

[10] R. del Campo, B. Savoini, A. Muñoz, M. A. Monge, and R. Pareja, “Processing and mechanical characteristics of magnesium-hydroxyapatite metal matrix biocomposites,” *J. Mech. Behav. Biomed. Mater.*, vol. 69, no. December 2016, pp. 135–143, 2017.

[11] M. Durisin, J. Reifenrath, C. M. Weber, R. Eifler, H. J. Maier, T. Lenarz, and J. M. Seitz, “Biodegradable nasal stents (MgF2-coated Mg–2 wt %Nd alloy)—A long-term in vivo study,” *J. Biomed. Mater. Res. - Part B Appl. Biomater.*, vol. 105, no. 2, pp. 350–365, 2017.

[12] A. Brown, S. Zaky, H. Ray, and C. Sfeir, “Porous magnesium/PLGA composite scaffolds for enhanced bone regeneration following tooth extraction,” *Acta Biomater.*, vol. 11, no. C, pp. 543–553, 2015.

[13] W. Liu, D. Zhai, Z. Huan, C. Wu, and J. Chang, “Novel tricalcium silicate/magnesium phosphate composite bone cement having high compressive strength, in vitro bioactivity and cytocompatibility,” *Acta Biomater.*, vol. 21, pp. 217–227, 2015.

[14] J. Zhang, X. Ma, D. Lin, H. Shi, Y. Yuan, W. Tang, H. Zhou, H. Guo, J. Qian, and C. Liu, “Magnesium modification of a calcium phosphate cement alters bone marrow stromal cell behavior via an integrin-mediated mechanism,” *Biomaterials*, vol. 53, pp. 251–264, 2015.

[15] S. Yoshizawa, A. Brown, A. Barchowsky, and C. Sfeir, “Magnesium ion stimulation of bone marrow stromal cells enhances osteogenic activity, simulating the effect of magnesium alloy degradation,” *Acta Biomater.*, vol. 10, no. 6, pp. 2834–2842, 2014.

[16] A. F. Cipriano, A. Sallee, R. Guan, Z. Zhao, M. Tayoba, J. Sanchez, and H. Liu, “Acta Biomaterialia Investigation of magnesium – zinc – calcium alloys and bone marrow derived mesenchymal stem cell response in direct culture,” *Acta Biomater.*, vol. 12, pp. 298–321, 2015.

[17] B. J. C. Luthringer and R. Willumeit-römer, “Effects of magnesium degradation products on mesenchymal stem cell fate and osteoblastogenesis,” *Gene*, vol. 575, no. 1, pp. 9–20, 2016.

[18] B. Kanter, A. Vikman, T. Brückner, M. Schamel, U. Gbureck, and A. Ignatius, “Bone regeneration capacity of magnesium phosphate cements in a large animal model,” *Acta Biomater.*, vol. 69, pp. 352–361, 2018.

[19] M. Nabiyouni, Y. Ren, and S. B. Bhaduri, “Magnesium substitution in the structure of orthopedic nanoparticles: A comparison between amorphous magnesium phosphates, calcium magnesium phosphates, and hydroxyapatites,” *Mater. Sci. Eng. C*, vol. 52, pp. 11–17, 2015.

[20] C. Chen, E. Karshalev, J. Guan, and J. Wang, “Magnesium-Based Micromotors: Water-Powered Propulsion, Multifunctionality, and Biomedical and Environmental Applications,” *Small*, vol. 14, no. 23, pp. 1–10, 2018.

[21] X. Huang, D. Wang, Z. Yuan, W. Xie, Y. Wu, R. Li, Y. Zhao, D. Luo, L. Cen, B. Chen, H. Wu, H. Xu, X. Sheng, M. Zhang, L. Zhao, and L. Yin, “A Fully Biodegradable Battery for Self-Powered Transient Implants,” *Small*, vol. 14, no. 28, pp. 1–8, 2018.

[22] Y. Yu, G. Jin, Y. Xue, D. Wang, X. Liu, and J. Sun, “Multifunctions of dual Zn/Mg ion co-implanted titanium on osteogenesis, angiogenesis and bacteria inhibition for dental implants,” *Acta Biomater.*, vol. 49, pp. 590–603, 2017.

[23] G. Wang, J. Li, W. Zhang, L. Xu, H. Pan, J. Wen, Q. Wu, W. She, T. Jiao, X. Liu, and X. Jiang, "Magnesium ion implantation on a micro / nanostructured titanium surface promotes its bioactivity and osteogenic differentiation function," pp. 2387–2398, 2014.

[24] World Health Organization and Food and Agriculture Organization of the United Nations, "Vitamin and mineral requirements in human nutrition Second edition," pp. 340–342, 2004.

[25] F. B. Hofmann, E. Board, J. a Beavo, a Busch, D. Ganten, M. C. Michel, C. P. Page, and W. Rosenthal, *Handbook of Experimental Pharmacology: Methylxanthines*. 2011.

[26] Y. Hashimoto, D. J. Kim, and J. C. Adams, "The roles of fascins in health and disease," *J. Pathol.*, vol. 224, no. 3, pp. 289–300, 2011.

[27] D. G. Barceloux and D. Barceloux, "Copper," *J. Toxicol. Clin. Toxicol.*, vol. 37, no. 2, pp. 217–230, Jan. 1999.

[28] D. G. Ellingsen, L. B. Møller, and J. Aaseth, "Copper," *Handb. Toxicol. Met. Fourth Ed.*, vol. 1, no. 29, pp. 765–786, 2015.

[29] F. Hofmann, E. Board, J. Beavo, D. Ganten, M. Michel, C. Page, and W. Rosenthal, *Handbook of Experimental Pharmacology 174*. 2008.

[30] F. H. Nielsen, "Importance of making dietary recommendations for elements designated as nutritionally beneficial, pharmacologically beneficial, or conditionally essential," *Journal of Trace Elements in Experimental Medicine*, vol. 13, no. 1. pp. 113–129, 2000.

[31] H. Busch, "Silicone toxicology," *Semin. Arthritis Rheum.*, vol. 24, no. 1 SUPPL. 1, pp. 11–17, 1994.

[32] D. Borenstein, "Siliconosis: A spectrum of illness," *Semin. Arthritis Rheum.*, vol. 24, no. 1 SUPPL. 1, pp. 1–7, 1994.

[33] R. J. Friedman, "Silicone breast prostheses implantation and explantation," *Semin. Arthritis Rheum.*, vol. 24, no. 1 SUPPL. 1, pp. 8–10, 1994.

[34] N. Kossovsky and J. Stassi, "A pathophysiological examination of the biophysics and bioreactivity of silicone breast implants," *Semin. Arthritis Rheum.*, vol. 24, no. 1 SUPPL. 1, pp. 18–21, 1994.

[35] S. Ivanov, S. Zhuravsky, G. Yukina, V. Tomson, D. Korolev, and M. Galagudza, "In vivo toxicity of intravenously administered silica and silicon nanoparticles," *Materials (Basel).*, vol. 5, no. 10, pp. 1873–1889, 2012.

[36] E. A. Ostrakhovitch, "Tin," in *Handbook on the Toxicology of Metals: Fourth Edition*, 4th Edit., vol. 1, Elsevier B.V., 2014, pp. 1241–1285.

[37] R. G. Lucchini, M. Aschner, Y. Kim, and M. Šarić, “Manganese,” in *Handbook on the Toxicology of Metals: Fourth Edition*, 4th Edit., vol. 1, Elsevier B.V., 2015, pp. 975–1011.

[38] J. S. Holler, B. A. Fowler, and G. F. Nordberg, “Silver,” in *Handbook on the Toxicology of Metals: Fourth Edition*, Fourth Edi., vol. 1, Elsevier, 2014, pp. 1209–1216.

[39] A. Bernard, “Lithium,” *Handb. Toxicol. Met. Fourth Ed.*, vol. 1, pp. 969–974, 2014.

[40] B. A. Fowler and N. Maples-Reynolds, “Indium,” in *Handbook on the Toxicology of Metals: Fourth Edition*, vol. 1, Elsevier B.V., 2015, pp. 845–853.

[41] European Food Safety Authority, *Tolerable Upper Intake Levels Scientific Committee on Food Scientific Panel on Dietetic Products, Nutrition and Allergies*, no. February. 2006.

[42] W. Querido, A. L. Rossi, and M. Farina, “The effects of strontium on bone mineral: A review on current knowledge and microanalytical approaches,” *Micron*, vol. 80, pp. 122–134, 2016.

[43] A. Bernard, “Lithium,” in *Handbook on the Toxicology of Metals*, Elsevier B.V., 2015, pp. 969–974.

[44] K. T. Rim, K. H. Koo, and J. S. Park, “Toxicological Evaluations of Rare Earths and Their Health Impacts to Workers : A Literature Review,” *Saf. Health Work*, vol. 4, no. 1, pp. 12–26, 2013.

[45] B. Sjögren, A. Iregren, J. Montelius, and R. A. Yokel, “Aluminum,” in *Handbook on the Toxicology of Metals*, 4th Edit., Elsevier B.V., 2015, pp. 549–564.

[46] A. Slikkerveer and F. A. de Wolff, “Pharmacokinetics and Toxicity of Bismuth Compounds,” *Med. Toxicol. Adverse Drug Exp.*, vol. 4, no. 5, pp. 303–323, 1989.

[47] J. S. Holler, B. A. Fowler, and G. F. Nordberg, “Silver,” in *Handbook on the Toxicology of Metals*, Fourth Edi., Elsevier B.V., 2015, pp. 1209–1216.

[48] E. A. Ostrakhovitch, “Tin,” in *Handbook on the Toxicology of Metals*, 4th Edit., Elsevier B.V., 2015, pp. 1241–1285.

[49] V. U. Blaschke C, “Soft and hard tissue response to zirconium dioxide dental implants: a clinical study in man. Neuro Endocrinol Lett. 2006;27 Suppl 1:69-72.,” *Neuro Endocrinol Lett. 2006;27 Suppl 1:69-72.*, vol. 27, no. Suppl 1, pp. 69–72, 2006.

[50] M. B. Greiter, A. Giussani, V. Höllriegl, W. B. Li, and U. Oeh, “Human biokinetic data and a new compartmental model of zirconium - a tracer study with enriched stable isotopes,” *Sci. Total Environ.*, vol. 409, no. 19, pp. 3701–3710, 2011.

[51] J. Hofstetter, E. Martinelli, A. M. Weinberg, M. Becker, B. Mingler, P. J.

Uggowitzer, and J. F. Löffler, “Assessing the degradation performance of ultrahigh-purity magnesium in vitro and in vivo,” *Corros. Sci.*, vol. 91, pp. 29–36, 2015.

[52] X. Gu, Y. Zheng, Y. Cheng, S. Zhong, and T. Xi, “Biomaterials In vitro corrosion and biocompatibility of binary magnesium alloys,” *Biomaterials*, vol. 30, no. 4, pp. 484–498, 2009.

[53] S. E. Harandi, M. Mirshahi, S. Koleini, M. H. Idris, H. Jafari, and M. R. A. Kadir, “Effect of calcium content on the microstructure, hardness and in-vitro corrosion behavior of biodegradable Mg-Ca binary alloy,” *Mater. Res.*, vol. 16, no. 1, pp. 11–18, 2013.

[54] R. Zeng, W. Qi, H. Cui, F. Zhang, S. Li, and E. Han, “In vitro corrosion of as-extruded Mg – Ca alloys — The influence of Ca concentration,” *Corros. Sci.*, vol. 96, pp. 23–31, 2015.

[55] J. W. Seong and W. J. Kim, “Development of biodegradable Mg-Ca alloy sheets with enhanced strength and corrosion properties through the refinement and uniform dispersion of the Mg2Ca phase by high-ratio differential speed rolling,” *Acta Biomater.*, vol. 11, no. 1, pp. 531–542, 2015.

[56] S. Zhang, X. Zhang, C. Zhao, J. Li, Y. Song, C. Xie, H. Tao, Y. Zhang, Y. He, Y. Jiang, and Y. Bian, “Research on an Mg-Zn alloy as a degradable biomaterial,” *Acta Biomater.*, vol. 6, no. 2, pp. 626–640, 2010.

[57] E. M. Salleh, H. Zuhailawati, S. N. F. Mohd Noor, and N. K. Othman, “In Vitro Biodegradation and Mechanical Properties of Mg-Zn Alloy and Mg-Zn-Hydroxyapatite Composite Produced by Mechanical Alloying for Potential Application in Bone Repair,” *Metall. Mater. Trans. A Phys. Metall. Mater. Sci.*, vol. 49, no. 11, pp. 5888–5903, 2018.

[58] J. cheng GAO, S. WU, L. ying QIAO, and Y. WANG, “Corrosion behavior of Mg and Mg-Zn alloys in simulated body fluid,” *Trans. Nonferrous Met. Soc. China (English Ed.*, vol. 18, no. 3, pp. 588–592, 2008.

[59] Y. Song, E. H. Han, D. Shan, C. D. Yim, and B. S. You, “The effect of Zn concentration on the corrosion behavior of Mg-xZn alloys,” *Corros. Sci.*, vol. 65, pp. 322–330, 2012.

[60] Y. Yan, H. Cao, Y. Kang, K. Yu, T. Xiao, J. Luo, Y. Deng, H. Fang, H. Xiong, and Y. Dai, “Effects of Zn concentration and heat treatment on the microstructure, mechanical properties and corrosion behavior of as-extruded Mg-Zn alloys produced by powder metallurgy,” *J. Alloys Compd.*, vol. 693, pp. 1277–1289, 2017.

[61] C. Liu, X. Fu, H. Pan, P. Wan, L. Wang, L. Tan, and K. Wang, “Biodegradable Mg-Cu alloys with enhanced osteogenesis , angiogenesis , and long-lasting antibacterial effects,” *Nat. Publ. Gr.*, no. May, pp. 1–17, 2016.

[62] X. Zhou, T. Guo, S. Wu, S. Lü, X. Yang, and W. Guo, “Effects of Si content and Ca

addition on thermal conductivity of As-Cast Mg-Si alloys," *Materials (Basel).*, vol. 11, no. 12, 2018.

[63] E. Zhang, L. Yang, J. Xu, and H. Chen, "Microstructure, mechanical properties and bio-corrosion properties of Mg-Si(-Ca, Zn) alloy for biomedical application," *Acta Biomater.*, vol. 6, no. 5, pp. 1756–1762, 2010.

[64] X. N. Gu, X. H. Xie, N. Li, Y. F. Zheng, and L. Qin, "In vitro and in vivo studies on a Mg-Sr binary alloy system developed as a new kind of biodegradable metal," *Acta Biomater.*, vol. 8, no. 6, pp. 2360–2374, 2012.

[65] Y. Wang, D. Tie, R. Guan, N. Wang, Y. Shang, T. Cui, and J. Li, "Microstructures, mechanical properties, and degradation behaviors of heat-treated Mg-Sr alloys as potential biodegradable implant materials," *J. Mech. Behav. Biomed. Mater.*, vol. 77, no. July 2017, pp. 47–57, 2018.

[66] S. Cai, T. Lei, N. Li, and F. Feng, "Effects of Zn on microstructure , mechanical properties and corrosion behavior of Mg – Zn alloys," *Mater. Sci. Eng. C*, vol. 32, no. 8, pp. 2570–2577, 2012.

[67] J. Peng, L. Zhong, Y. Wang, Y. Lu, and F. Pan, "Effect of extrusion temperature on the microstructure and thermal conductivity of Mg-2.0Zn-1.0Mn-0.2Ce alloys," *Mater. Des.*, vol. 87, no. December 2015, pp. 914–919, 2015.

[68] C. J. Boehlert and K. Knittel, "The microstructure, tensile properties, and creep behavior of Mg-Zn alloys containing 0-4.4 wt.% Zn," *Mater. Sci. Eng. A*, vol. 417, no. 1–2, pp. 315–321, 2006.

[69] N. El Mahallawy, A. Ahmed Diaa, M. Akdesir, and H. Palkowski, "Effect of Zn addition on the microstructure and mechanical properties of cast, rolled and extruded Mg-6Sn-xZn alloys," *Mater. Sci. Eng. A*, vol. 680, no. October 2016, pp. 47–53, 2017.

[70] Y. C. Lee, A. K. Dahle, and D. H. Stjohn, "The role of solute in grain refinement of magnesium," *Metall. Mater. Trans. A Phys. Metall. Mater. Sci.*, vol. 31, no. 11, pp. 2895–2906, 2000.

[71] Z. Li, X. Gu, S. Lou, and Y. Zheng, "The development of binary Mg-Ca alloys for use as biodegradable materials within bone," *Biomaterials*, vol. 29, no. 10, pp. 1329–1344, 2008.

[72] H. R. B. Rad, M. H. Idris, M. R. A. Kadir, and S. Farahany, "Microstructure analysis and corrosion behavior of biodegradable Mg-Ca implant alloys," *Mater. Des.*, vol. 33, no. 1, pp. 88–97, 2012.

[73] W. Wang, J. Han, X. Yang, M. Li, P. Wan, L. Tan, Y. Zhang, and K. Yang, "Novel biocompatible magnesium alloys design with nutrient alloying elements Si, Ca and Sr: Structure and properties characterization," *Mater. Sci. Eng. B*, vol. 214, pp. 26–36, 2016.

[74] Y. Li, L. Liu, P. Wan, Z. Zhai, Z. Mao, Z. Ouyang, D. Yu, Q. Sun, L. Tan, L. Ren, Z. Zhu, Y. Hao, X. Qu, K. Yang, and K. Dai, "Biodegradable Mg-Cu alloy implants with antibacterial activity for the treatment of osteomyelitis: In vitro and in vivo evaluations," *Biomaterials*, vol. 106, pp. 250–263, 2016.

[75] M. Lotfpour, M. Emamy, C. Dehghanian, and K. Tavighi, "Influence of Cu Addition on the Structure , Mechanical and Corrosion Properties of Cast Mg-2 % Zn Alloy," *J. Mater. Eng. Perform.*, vol. 26, no. 5, pp. 2136–2150, 2017.

[76] L. Čížek, A. Hanus, O. Blahož, T. Tański, L. A. Dobrzański, M. Praźmowski, and L. Pawlica, "Structure and mechanical properties of Mg-Si alloys at elevated temperatures," *J. Achiev. Mater. Manuf. Eng.*, vol. 35, no. 1, pp. 37–46, 2009.

[77] J. Zheng, Q. Wang, Z. Jin, and T. Peng, "The microstructure, mechanical properties and creep behavior of Mg-3Sm-0.5Zn-0.4Zr (wt.%) alloy produced by different casting technologies," *J. Alloys Compd.*, vol. 496, no. 1–2, pp. 351–356, 2010.

[78] C. Zhao, F. Pan, S. Zhao, H. Pan, K. Song, and A. Tang, "Microstructure, corrosion behavior and cytotoxicity of biodegradable Mg-Sn implant alloys prepared by sub-rapid solidification," *Mater. Sci. Eng. C*, vol. 54, pp. 245–251, 2015.

[79] E. Willbold, K. Kalla, I. Bartsch, K. Bobe, M. Brauneis, S. Remennik, D. Shechtman, J. Nellesen, W. Tillmann, C. Vogt, and F. Witte, "Biocompatibility of rapidly solidified magnesium alloy RS66 as a temporary biodegradable metal," *Acta Biomater.*, vol. 9, no. 10, pp. 8509–8517, 2013.

[80] Y. Huang, D. Liu, L. Anguilano, C. You, and M. Chen, "Fabrication and characterization of a biodegradable Mg-2Zn-0.5Ca/1β-TCP composite," *Mater. Sci. Eng. C*, vol. 54, pp. 120–132, 2015.

[81] D. J. Lin, F. Y. Hung, T. S. Lui, and M. L. Yeh, "Heat treatment mechanism and biodegradable characteristics of ZAX1330 Mg alloy," *Mater. Sci. Eng. C*, vol. 51, pp. 300–308, 2015.

[82] D. Dziuba, A. Meyer-Lindenberg, J. M. Seitz, H. Waizy, N. Angrisani, and J. Reifenrath, "Long-term in vivo degradation behaviour and biocompatibility of the magnesium alloy ZEK100 for use as a biodegradable bone implant," *Acta Biomater.*, vol. 9, no. 10, pp. 8548–8560, 2013.

[83] P. Poddar, S. Bagui, K. Ashok, and A. P. Murugesan, "Experimental investigation on microstructure and mechanical properties of gravity-die-cast magnesium alloys," *J. Alloys Compd.*, vol. 695, pp. 895–908, 2017.

[84] J. Su, M. Sanjari, A. S. H. Kabir, I. H. Jung, J. J. Jonas, S. Yue, and H. Utsunomiya, "Characteristics of magnesium AZ31 alloys subjected to high speed rolling," *Mater. Sci. Eng. A*, vol. 636, no. June, pp. 582–592, 2015.

[85] H. Asgharzadeh, E. Y. Yoon, H. J. Chae, T. S. Kim, J. W. Lee, and H. S. Kim, "Microstructure and mechanical properties of a Mg-Zn-Y alloy produced by a

powder metallurgy route," *J. Alloys Compd.*, vol. 586, no. SUPPL. 1, pp. S95–S100, 2014.

[86] J. Kubásek, D. Dvorský, M. Čavojský, D. Vojtěch, N. Beronská, and M. Fousová, "Superior Properties of Mg–4Y–3RE–Zr Alloy Prepared by Powder Metallurgy," *J. Mater. Sci. Technol.*, vol. 33, no. 7, pp. 652–660, 2017.

[87] M. Rashad, F. Pan, and M. Asif, "Room temperature mechanical properties of Mg-Cu-Al alloys synthesized using powder metallurgy method," *Mater. Sci. Eng. A*, vol. 644, pp. 129–136, 2015.

[88] J. Feng, H. Sun, X. Li, J. Zhang, W. Fang, and W. Fang, "Microstructures and mechanical properties of the ultrafine-grained Mg-3Al-Zn alloys fabricated by powder metallurgy," *Adv. Powder Technol.*, vol. 27, no. 2, pp. 550–556, 2016.

[89] T. Zhou, M. Yang, Z. Zhou, J. Hu, and Z. Chen, "Microstructure and mechanical properties of rapidly solidified/powder metallurgy Mg-6Zn and Mg-6Zn-5Ca at room and elevated temperatures," *J. Alloys Compd.*, vol. 560, pp. 161–166, 2013.

[90] T. Zhou, H. Xia, M. Yang, Z. Zhou, K. Chen, J. Hu, and Z. Chen, "Investigation on microstructure characterizations and phase compositions of rapidly solidification/powder metallurgy Mg-6 wt.% Zn-5 wt.% Ce-1.5 wt.% Ca alloy," *J. Alloys Compd.*, vol. 509, no. 9, pp. L145–L149, 2011.

[91] I. Stulikova, B. Smola, M. Vlach, H. Kudrnova, and J. Piesova, "Influence of powder metallurgy route on precipitation processes in MgTbNd alloy," *Mater. Charact.*, vol. 112, pp. 149–154, 2016.

[92] J. She, F. Pan, J. Zhang, A. Tang, S. Luo, Z. Yu, K. Song, and M. Rashad, "Microstructure and mechanical properties of Mg-Al-Sn extruded alloys," *J. Alloys Compd.*, vol. 657, pp. 893–905, 2016.

[93] G. S. Hu, D. F. Zhang, D. Z. Zhao, X. Shen, L. Y. Jiang, and F. S. Pan, "Microstructures and mechanical properties of extruded and aged Mg-Zn-Mn-Sn-Y alloys," *Trans. Nonferrous Met. Soc. China (English Ed.*, vol. 24, no. 10, pp. 3070–3075, 2014.

[94] H. Y. Ha, J. Y. Kang, S. G. Kim, B. Kim, S. S. Park, C. D. Yim, and B. S. You, "Influences of metallurgical factors on the corrosion behaviour of extruded binary Mg-Sn alloys," *Corros. Sci.*, vol. 82, pp. 369–379, 2014.

[95] D. Chen, Y. P. Ren, Y. Guo, W. L. Pei, H. Da Zhao, and G. W. Qln, "Microstructures and tensile properties of as-extruded Mg-Sn binary alloys," *Trans. Nonferrous Met. Soc. China (English Ed.*, vol. 20, no. 7, pp. 1321–1325, 2010.

[96] W. L. Cheng, S. S. Park, B. S. You, and B. H. Koo, "Microstructure and mechanical properties of binary Mg-Sn alloys subjected to indirect extrusion," *Mater. Sci. Eng. A*, vol. 527, no. 18–19, pp. 4650–4653, 2010.

[97] S. F. Hassan, O. O. Nasirudeen, N. Al-Aqeeli, N. Saheb, F. Patel, and M. M. A.

Baig, “Magnesium-nickel composite: Preparation, microstructure and mechanical properties,” *J. Alloys Compd.*, vol. 646, pp. 333–338, 2015.

[98] S. F. Hassan, K. S. Tun, and M. Gupta, “Effect of sintering techniques on the microstructure and tensile properties of nano-yttria particulates reinforced magnesium nanocomposites,” *J. Alloys Compd.*, vol. 509, no. 11, pp. 4341–4347, 2011.

[99] S. F. Hassan, O. Siddiqui, M. F. Ahmed, and A. I. Al Nawwah, “Development of Gradient Concentrated Single-Phase Fine Mg-Zn Particles and Effect on Structure and Mechanical Properties,” *J. Eng. Mater. Technol.*, vol. 141, no. 2, p. 021007, 2018.

[100] S. F. Hassan, K. S. Tun, F. Patel, N. Al-Aqeeli, and M. Gupta, “NICKELIZATION EFFECT ON THE HIGH TEMPERATURE TENSILE PROPERTIES OF Mg-0.7Y2O3 NANOCOMPOSITE,” *Arch. Metall. Mater.*, vol. 63, no. 3, pp. 1411–1415, 2018.

[101] S. F. Hassan, M. J. Tan, and M. Gupta, “ Development of nano-ZrO 2 reinforced magnesium nanocomposites with significantly improved ductility ,” *Mater. Sci. Technol.*, vol. 23, no. 11, pp. 1309–1312, 2007.

[102] F. Cardarelli, *Materials Handbook*. Cham: Springer International Publishing, 2018.

[103] O. Sitdikov and R. Kaibyshev, “Dynamic Recrystallization in Pure Magnesium,” *Mater. Trans.*, vol. 42, no. 9, pp. 1928–1937, 2001.

[104] F. C. Campbell, *Elements of Metallurgy and Engineering Alloys*, vol. Materials (Basel). ASM International, 2008.

[105] ASM International. Handbook Committee, *ASM Handbook Volume 3 - Alloy Phase Diagrams*. 1992.

[106] J. Dai, B. Jiang, J. Zhang, Q. Yang, Z. Jiang, H. Dong, and F. Pan, “Diffusion Kinetics in Mg-Cu Binary System,” *J. Phase Equilibria Diffus.*, vol. 36, no. 6, pp. 613–619, 2015.

[107] H. Mehrer and S. V. Divinski, “Diffusion in Metallic Elements and Intermetallics,” *Defect Diffus. Forum*, vol. 289–292, no. November, pp. 15–38, 2009.

[108] S. Fida Hassan, M. T. Islam, S. Nouari, N. Al-Aqeeli, M. M. A. Baig, and F. Patel, “Mg6Zn0.4Ca0.5Cu alloy: Physically blended microalloyed lightweight alloy with significantly high strength and ductility,” *J. Alloys Compd.*, vol. 787, pp. 1015–1022, 2019.

[109] K. S. Tun and M. Gupta, “Role of microstructure and texture on compressive strength improvement of Mg/(Y2O3 + Cu) hybrid nanocomposites,” *J. Compos. Mater.*, vol. 44, no. 25, pp. 3033–3050, 2010.

APPENDIX

Binary Phase Diagrams

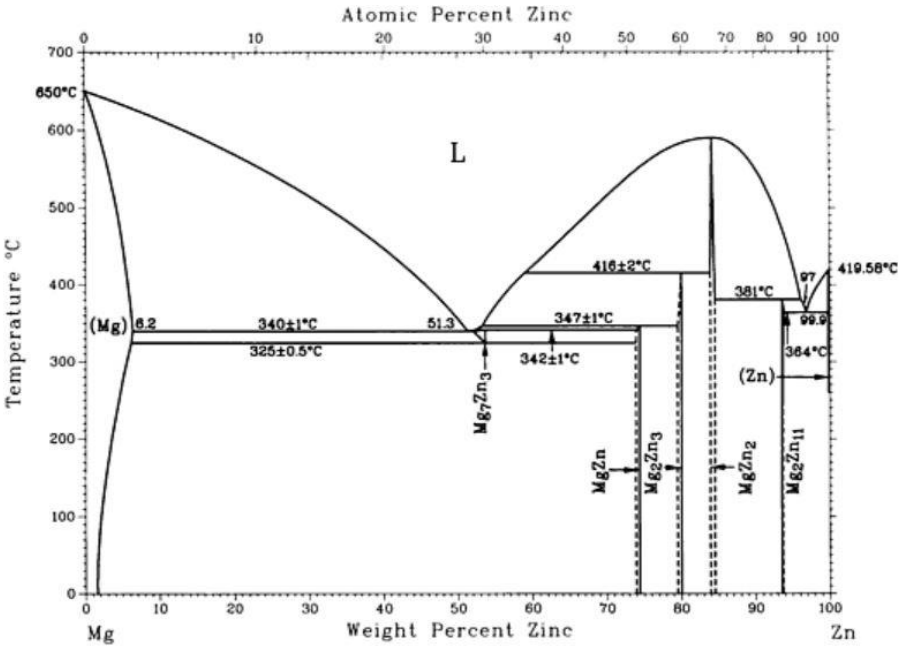

Figure 37: Binary Phase diagram of Mg-Zn [105].

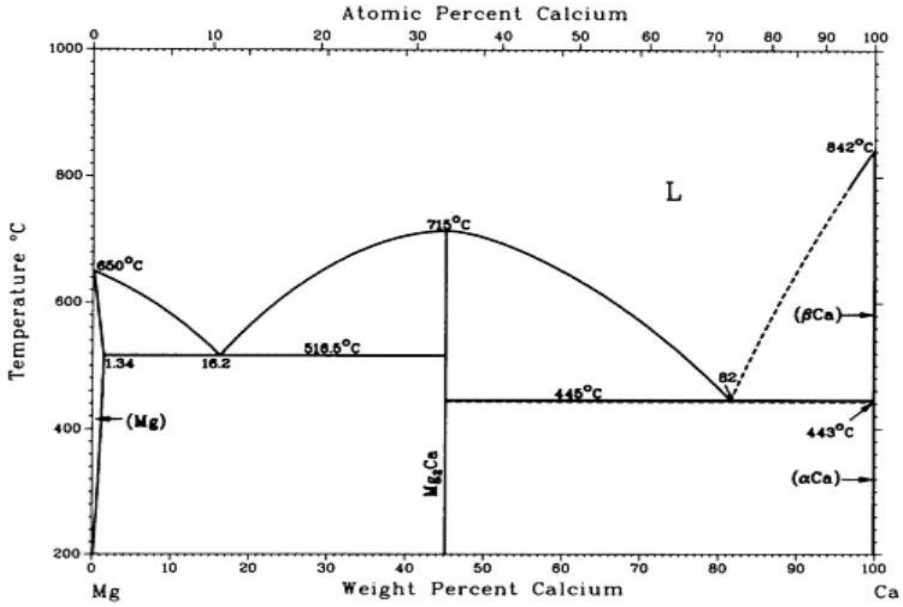

Figure 38: Binary Phase diagram of Mg-Ca [105].

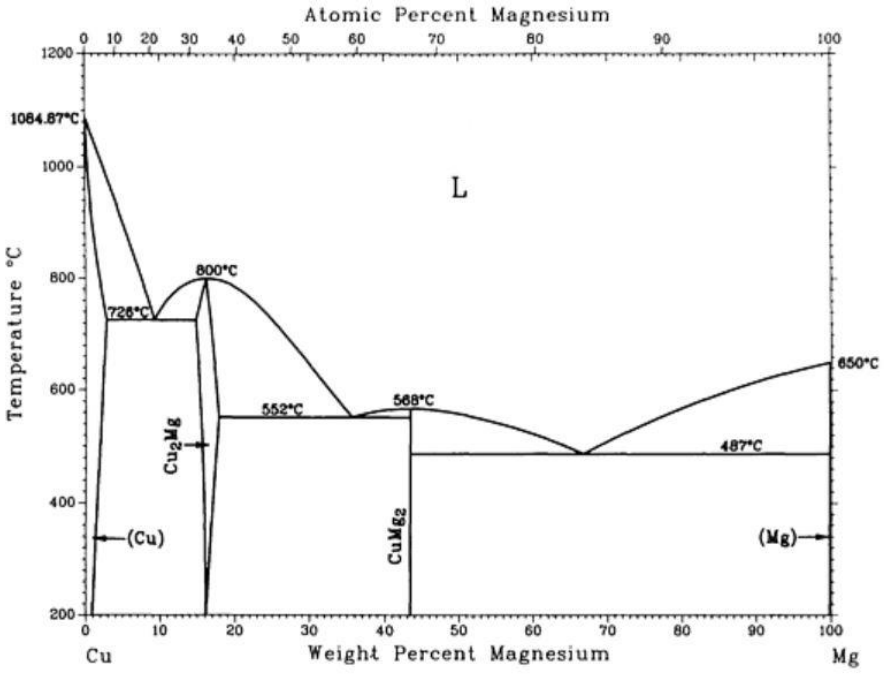

Figure 39: Binary Phase diagram of Mg-Cu [105].

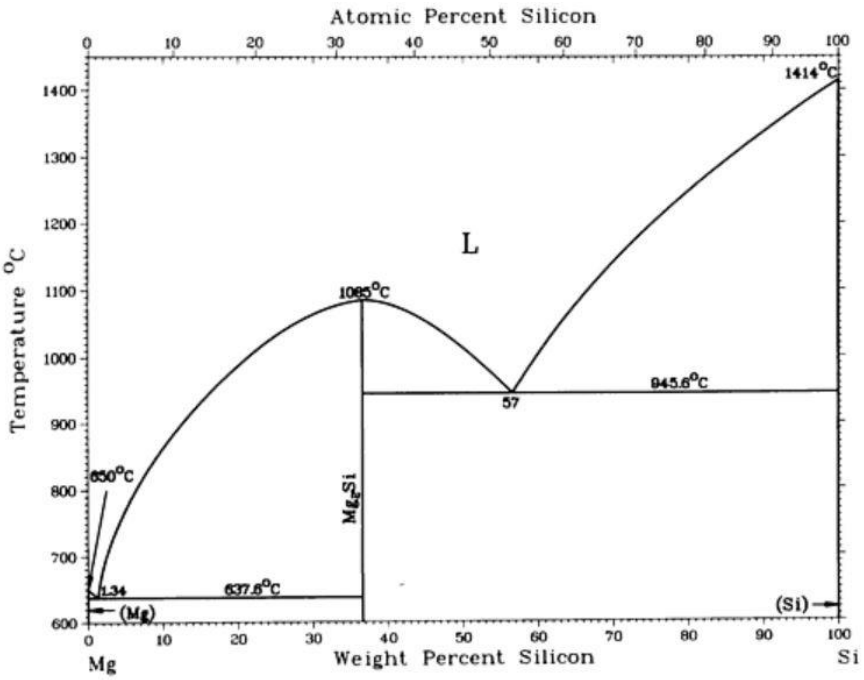

Figure 40: Binary Phase diagram of Mg-Si [105].

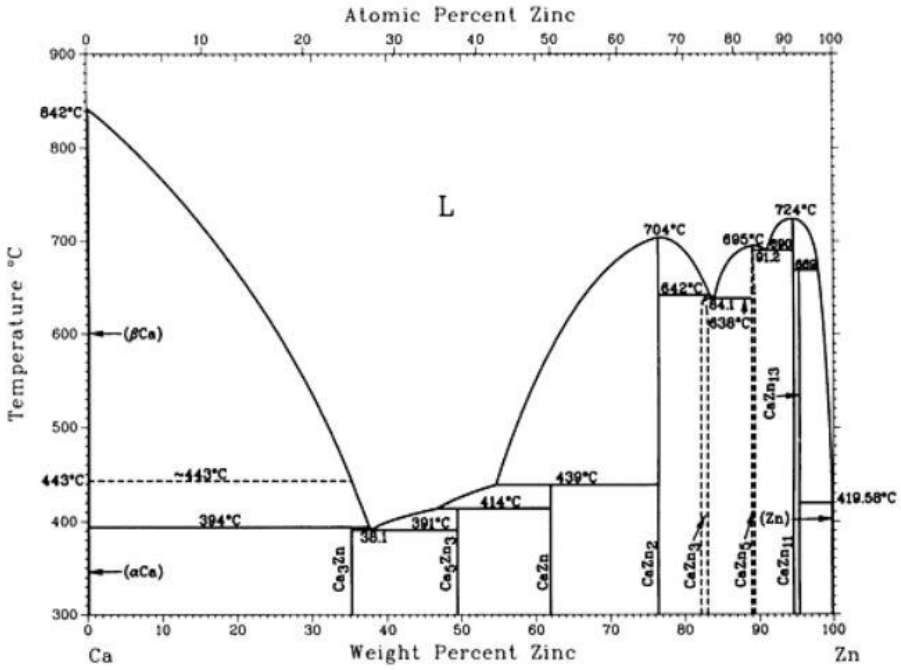

Figure 41: Binary Phase diagram of Ca-Zn [105].

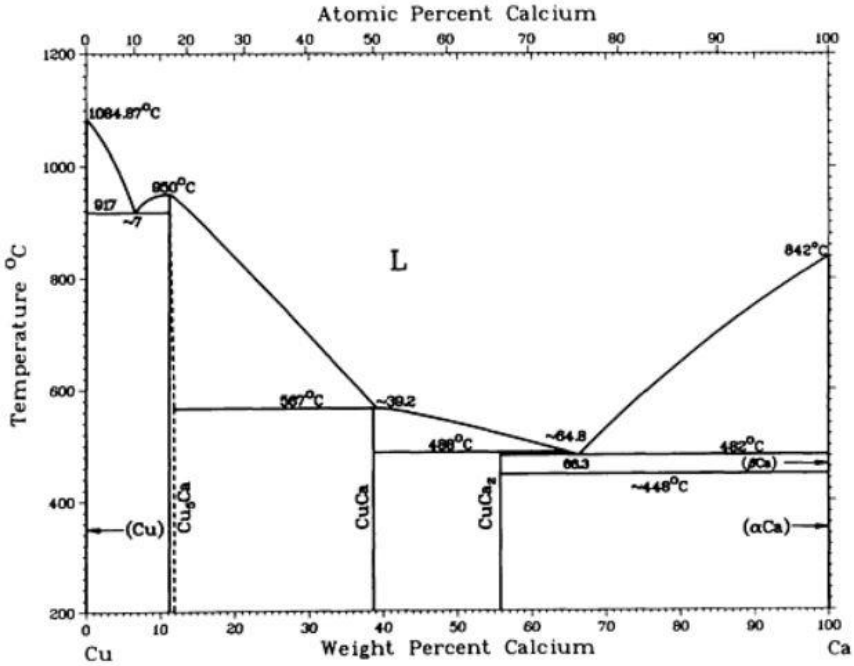

Figure 42: Binary Phase diagram of Ca-Cu [105].

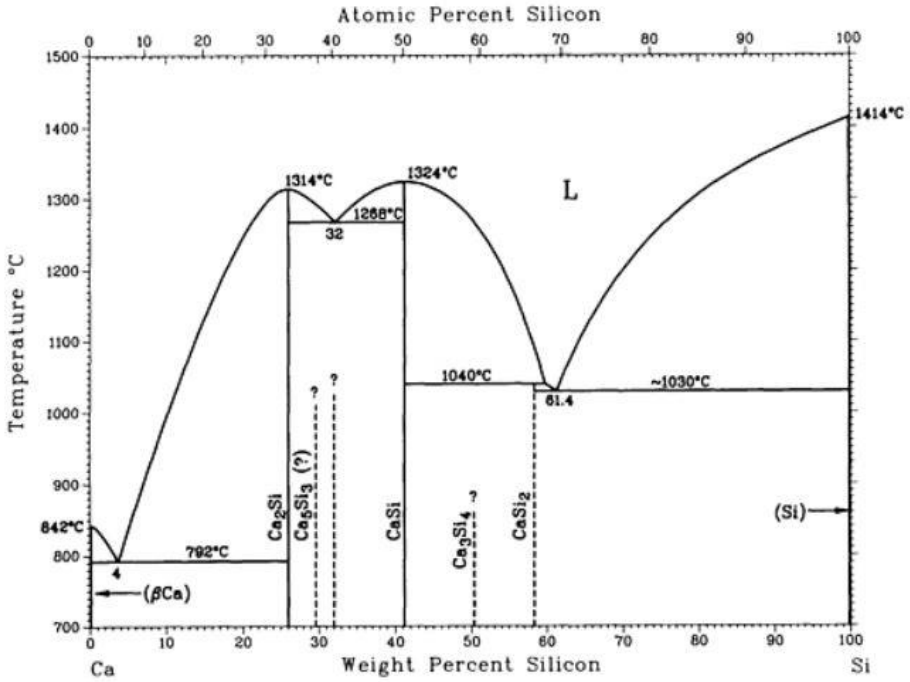

Figure 43: Binary Phase diagram of Ca-Si [105].

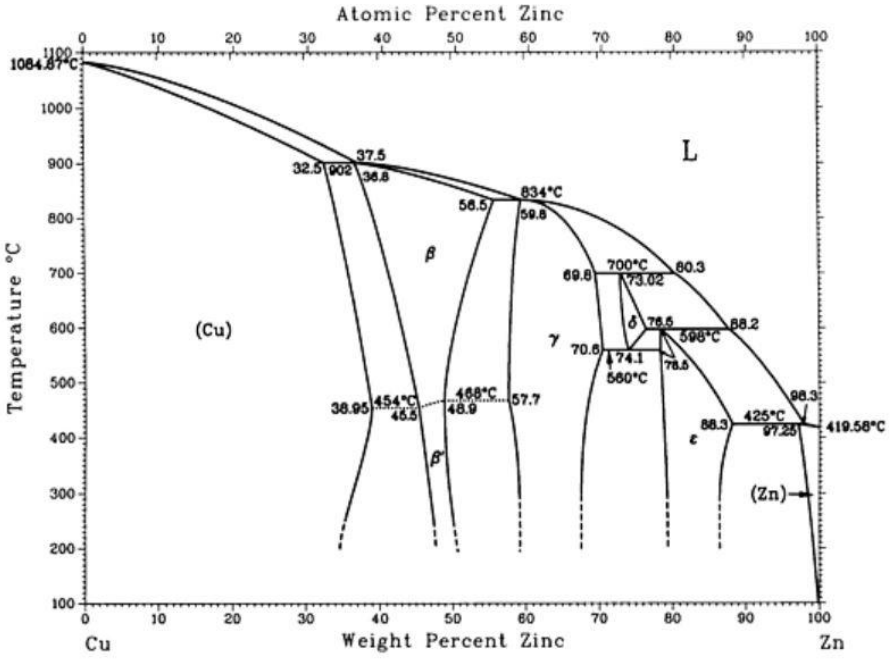

Figure 44: Binary Phase diagram of Cu-Zn [105].

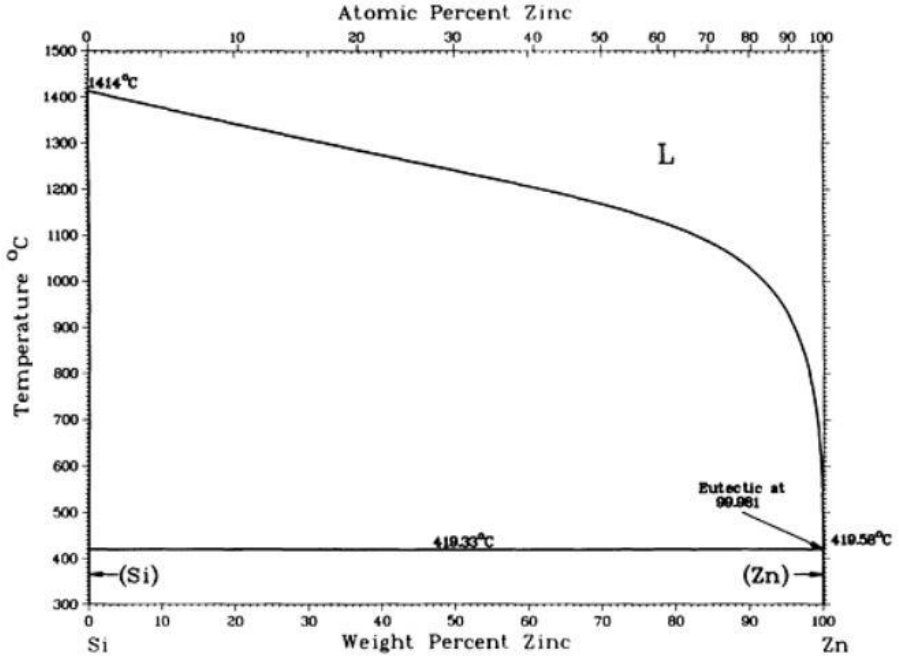

Figure 45: Binary Phase diagram of Si-Zn [105].

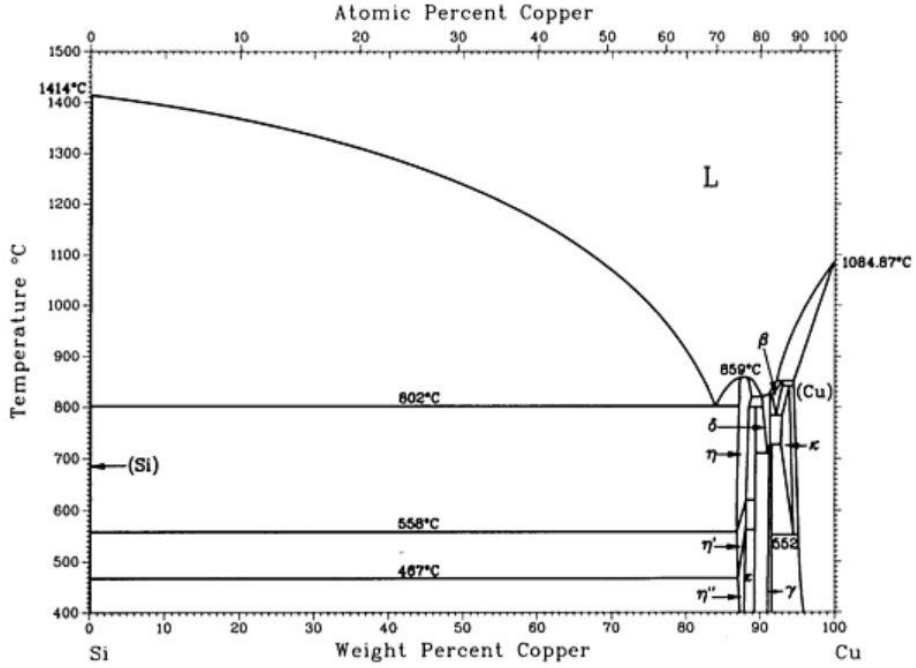

Figure 46: Binary Phase diagram of Si-Cu [105].

Vitae

Name :Mir Thaufeequl Islam

Nationality :Maldivian

Date of Birth :7/12/1987

Email :mirthaufeeq@gmail.com

Address :Maldives

Academic Background :Bachelor of Science in Mechanical Engineering (2012), Islamic University of Technology (IUT- an organ of Organization of Islamic Co-operation), Bangladesh.